

General Disclaimer

One or more of the Following Statements may affect this Document

- This document has been reproduced from the best copy furnished by the organizational source. It is being released in the interest of making available as much information as possible.
- This document may contain data, which exceeds the sheet parameters. It was furnished in this condition by the organizational source and is the best copy available.
- This document may contain tone-on-tone or color graphs, charts and/or pictures, which have been reproduced in black and white.
- This document is paginated as submitted by the original source.
- Portions of this document are not fully legible due to the historical nature of some of the material. However, it is the best reproduction available from the original submission.

(NASA-CR-174210) PRECISE CONTROL OF
FLEXIBLE MANIPULATORS Final Report, Mar.
1983 - Jun. 1984 (Stanford Univ.) 53 p
HC A04/MF A01

N85-16178

CSCL 05H

Unclas

G3/37 01370

FINAL REPORT
for the period
March 1983 to June 1984

RESEARCH GRANT NO. NAG 1-322

PRECISE CONTROL OF FLEXIBLE MANIPULATORS

submitted to

**NATIONAL AERONAUTICS AND SPACE ADMINISTRATION
LANGLEY RESEARCH CENTER, HAMPTON, VA 23665**

Principal investigators:
Professor Robert H. Cannon, Jr.
Professor Thomas O. Binford

Stanford University
Stanford, California 94305

Prepared by: Eric Schmits
September 1984

ORIGINAL CONTAINS
COLOR ILLUSTRATIONS

FINAL REPORT
for the period
March 1983 to June 1984

RESEARCH GRANT NO. NAG 1-322

PRECISE CONTROL OF FLEXIBLE MANIPULATORS

submitted to

**NATIONAL AERONAUTICS AND SPACE ADMINISTRATION
LANGLEY RESEARCH CENTER, HAMPTON, VA 23665**

Principal Investigators:
Professor Robert H. Cannon, Jr.
Professor Thomas O. Bindford

Stanford University
Stanford, California 94305

Prepared by: Eric Schmitz
September 1984

Contents

	Page
Summary	1
1 Introduction	2
2 Experimental set-up and dynamic modelling	2
2.1 Experimental set-up	6
2.2 Dynamic modelling.	8
3 Joint angle versus end-point position feedback.	10
3.1 Conventional joint angle feedback.	10
3.1.1 Design	10
3.1.2 Experimental results	13
3.2 End-point feedback control.	15
3.2.1 Design	15
3.2.2 Experimental results	15
4 LQG design and performance.	18
4.1 Regulator design	19
4.2 Continuous estimator design	19
4.3 Closed-loop performance	23
4.3.1 Step response command	23
4.3.2 Disturbance response	25
4.3.3 Robustness	26
5 Low-order compensator	29
5.1 Description of the design algorithm	29
5.2 Design procedure	30
5.3 Design #1	30
5.4 Design #2	32
5.5 Experimental verification	32
5.5.1 Implementation	32
5.5.2 Closed-loop response	34
6 Switching between sensor sets.	34
6.1 Motivation.	34
6.2 Proposed solution	36
6.3 Design of the estimator	36
6.4 Regulator and slew command profile	38
6.5 Experimental results	38
7 Conclusion	39

Appendix A Flexible arm open-loop transfer functions.	41
Appendix B Locus of asymptotic estimator poles	42
Appendix C Transfer function calculations	44
Appendix D Discrete LQG compensator implementation and check-out	46
1 LQG compensator implementation.	46
2 Compensator check-out	48

Summary

ORIGINAL CONTAINS
COLOR ILLUSTRATIONS

This report summarizes the design and experimental testing of end-point position controllers for a very flexible one-link lightweight manipulator.

First, we describe the latest upgraded version of the experimental set-up.

Second, we discuss the basic differences between conventional joint-angle feedback (as used for today's manipulators) and end-point position feedback.

In the third part, we outline a general procedure for applying modern control methods (steady-state LQG design) to the problem at hand. The main difficulty with LQG design methods is to choose appropriate values for the weighting parameters that are used in the performance index to be minimized. We show in this report the relation between these parameters and the bandwidth and control stiffness of the resulting end-point position closed-loop system. An important result obtained via the modern control design is that joint rate angle feedback in addition to the primary end-point position sensor is essential for adequate disturbance rejection capability of the closed-loop system.

In the next section, we document results on the use of a low-order multivariable compensator design computer code, called "Sandy". A fourth-order compensator was successfully demonstrated on the experimental arm, with similar performance to the one for the LQG 9th order compensator.

The last section outlines a solution to the problem of control mode switching between position sensor sets. This method requires the use of a full-order LQG controller.

As a general conclusion, the proof of concept for end-point position feedback for a one link flexible manipulator has been demonstrated in the laboratory. The bandwidth obtained with the experimental end-point position controller is about twice as fast as the beam's first natural cantilevered frequency, and comes within a factor of four of the absolute physical speed limit imposed by the wave propagation time of the beam. The next logical step is to extend this new capability to multi-link flexible manipulators.

1 Introduction

The research reported in this report is a laboratory demonstration of feedback control schemes for fast and accurate end-point positioning of a single link light-weight and very flexible manipulator. The central problem addressed here is the problem of controlling the end-point (hand) of a manipulator by measuring its position at that point and using that measurement to apply a control torque with an actuator at the other end of the flexible manipulator. With a light-weight manipulator and end-point sensing, we can achieve both high speed motion and fast vibration settling times.

Research on elastic manipulators has been concerned so far mostly with the difficult dynamic modelling problem [11],[12],[15],[18]. Control schemes for elastic manipulators are still in their first stages of development [11],[16],[17],[18],[19]. Note also that there is some common ground between the development of control algorithms for large space flexible structures [22],[23],[24],[25] and for elastic manipulators .

The best example of an existing very flexible manipulator is the Space Shuttle Remote Manipulator System, developed and built by Spar Aerospace Inc. for NASA. Its first cantilevered vibration frequency with all joints locked is in the range of 0.04 Hz to 0.35 Hz, depending on the payload [13],[14]. It uses a conventional independent joint servocontrol, and it moves relatively slowly (0.5 deg/sec) so as to minimize the elastic deformations. It is expected that a variety of new manipulators will be developed as part of the Space Station project under NASA direction. Among other things, manipulators can be used in space as aids for space-structures assembly and for many specialized tasks such as in-orbit satellite repair and refueling [21].

This report extends the results given in [1]. After a brief review of the experimental set-up and of the dynamic modelling, the next three sections cover the position control design problem: (1) basic differences between joint angle and end-point feedback for some simple feedback laws. (2) design of a high performance tip position controller using the modern control approach (Linear Quadratic Gaussian design). (3) application of a design method to reduce the 9th order LQG compensators to simpler 4th order compensators.

Finally, a new problem specific to elastic manipulators, namely control mode switching between end-point and joint angle sensors is discussed.

2 Experimental set-up and dynamic modelling

In this section, we describe the latest hardware and software implementations and then we recapitulate the dynamic model used for control design.

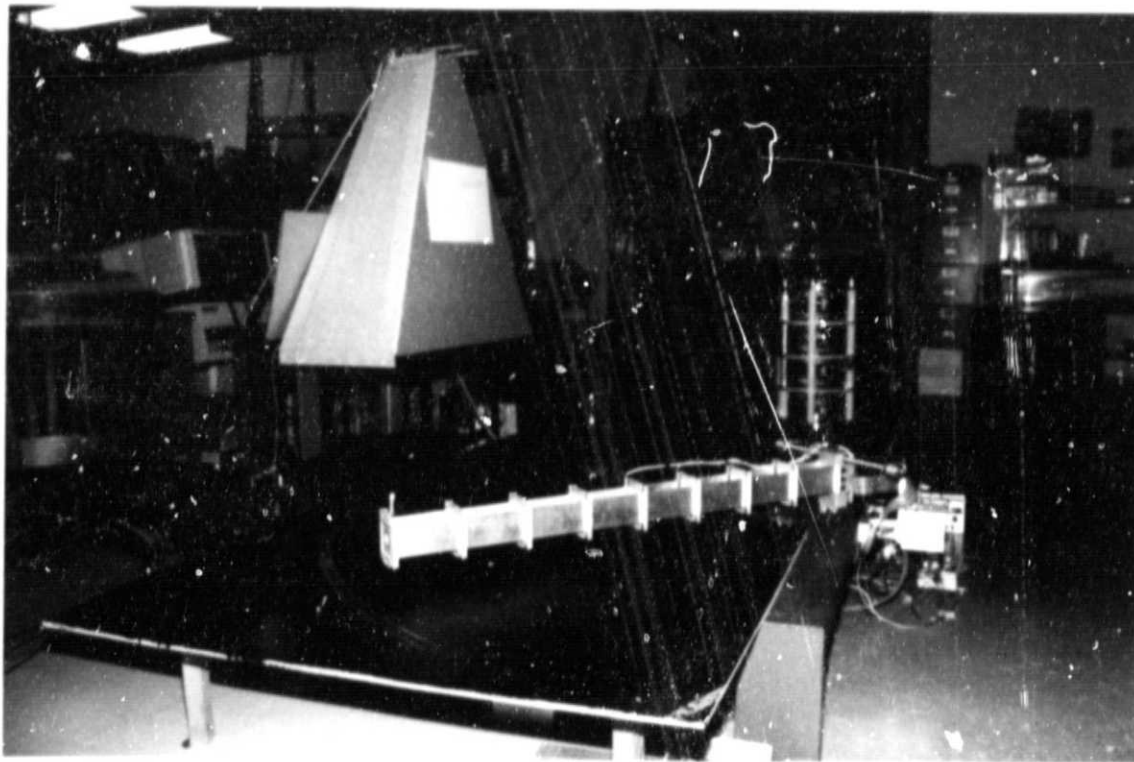


Fig. 2.1 Overview of the experimental flexible arm (1):
the large hood prevents the background light from disturbing the end-point photosensor.

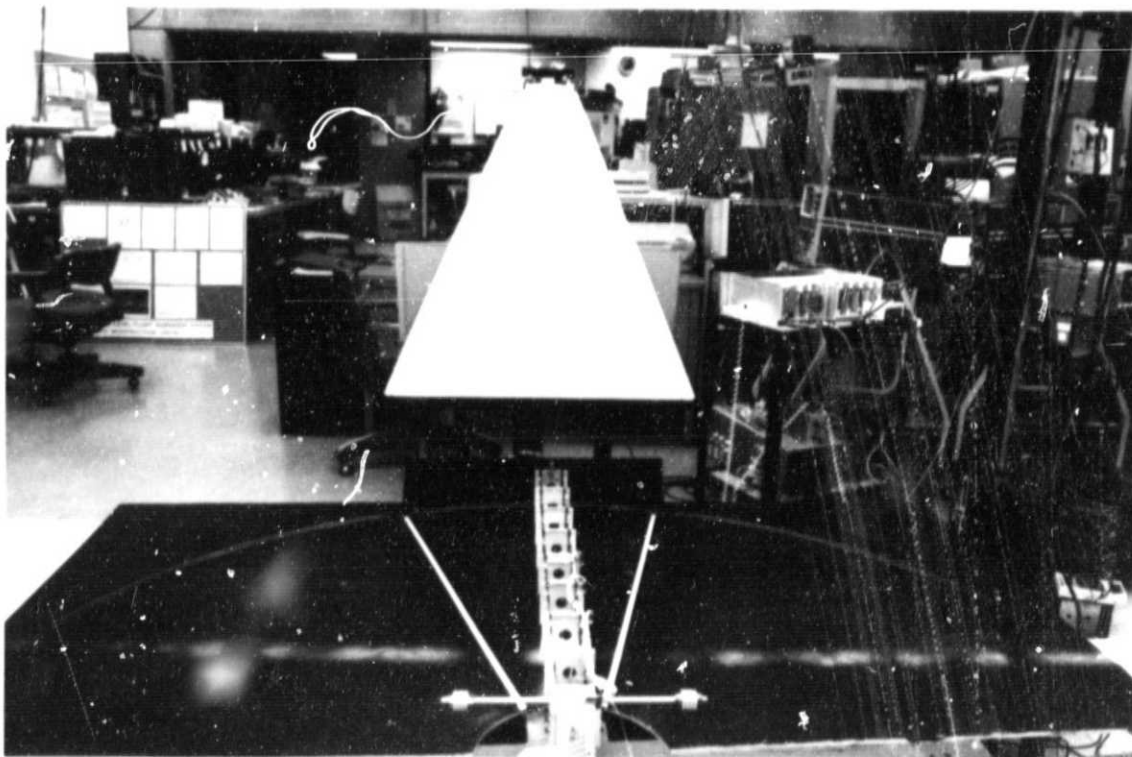


Fig. 2.2 Overview of the experimental flexible arm (2):
the analog amplifiers rack, the actuator power amplifier and the MINC 11 DEC laboratory computer can be seen on the right side of this picture.

ORIGINAL PHOTO
COLOR REPRODUCTION

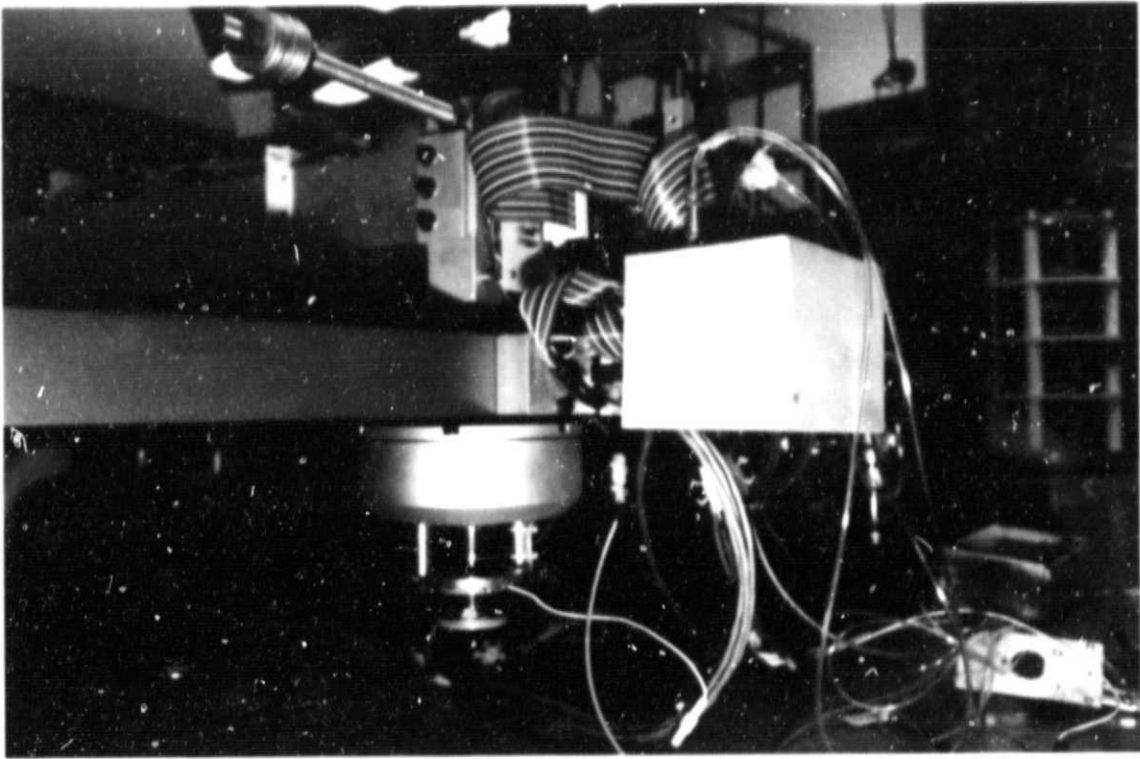


Fig. 2.3 View of the Aeroflex brushless limited angle torque motor:
the lower end of the shaft is connected to a film wire potentiometer. The arm
hub is clamped to the upper end of the shaft.

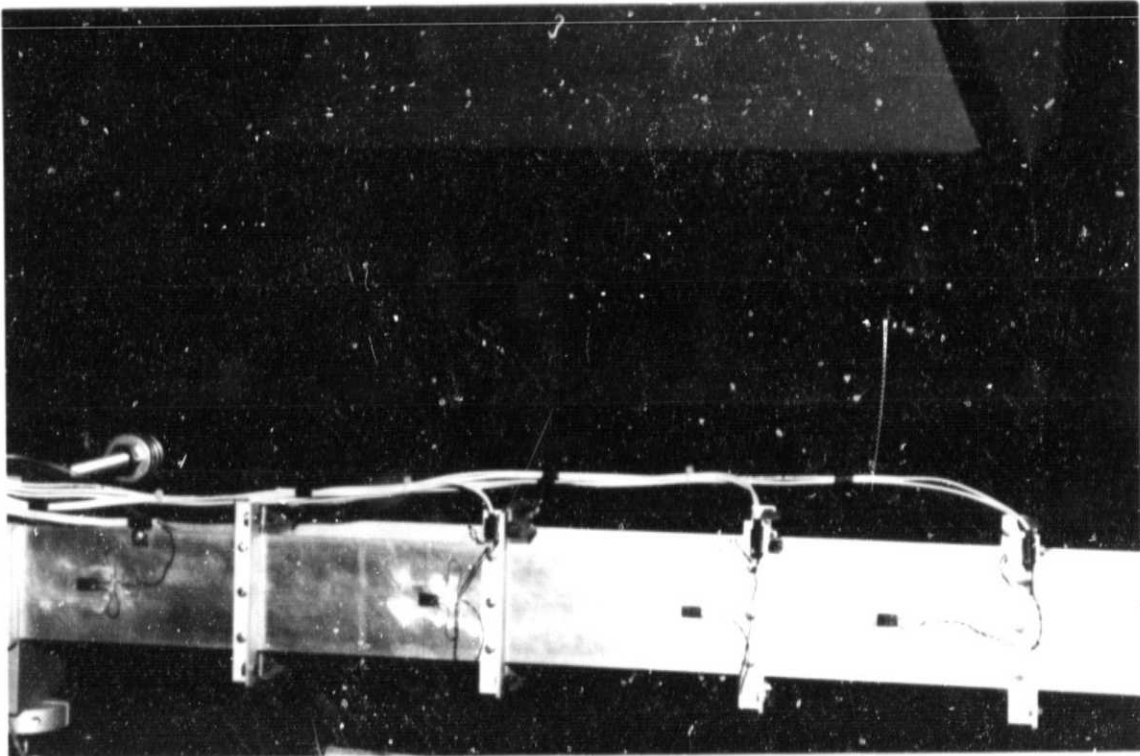


Fig. 2.4 View of the strain-gauges :
they are glued on each side of the right beam. The strain-gauge positioned
the closest to the hub (left side of the picture) is used for active feedback
control.

ORIGINAL PAGE
COLOR PHOTOGRAPH

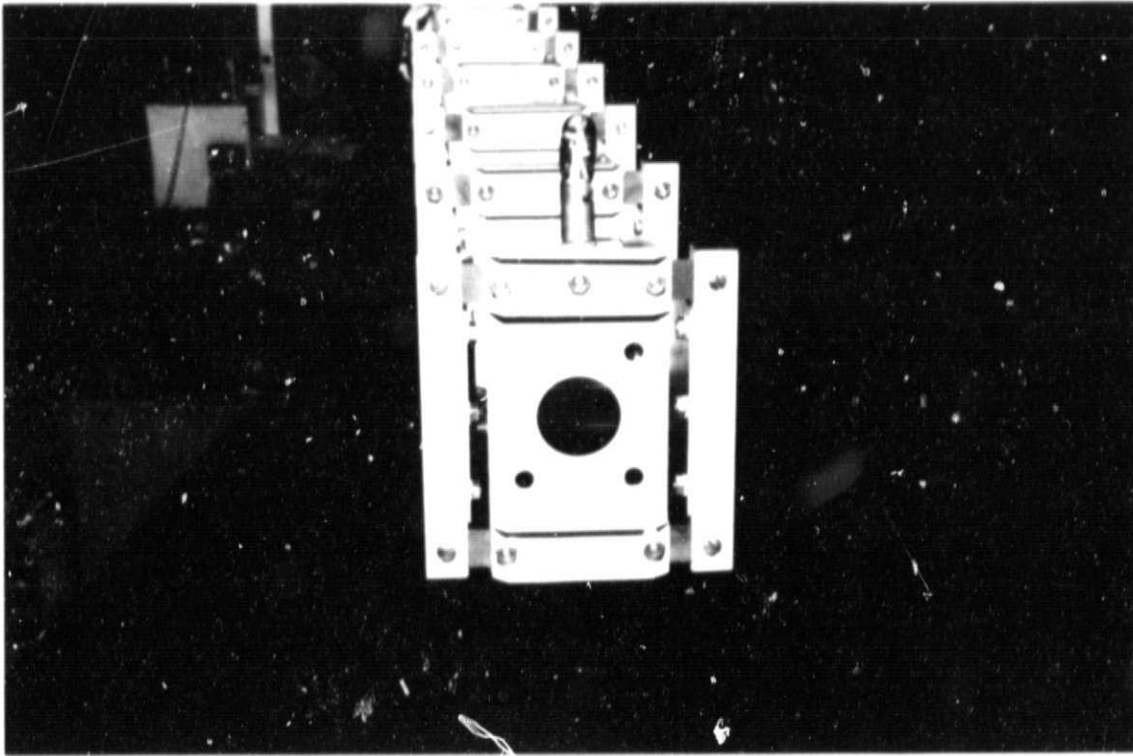


Fig. 2.5 Front view of the arm from the tip:

the last bridge with its hardened beryllium copper flex joints (in dark on the picture) is also used as a mount for the light source detected by the photosensor.

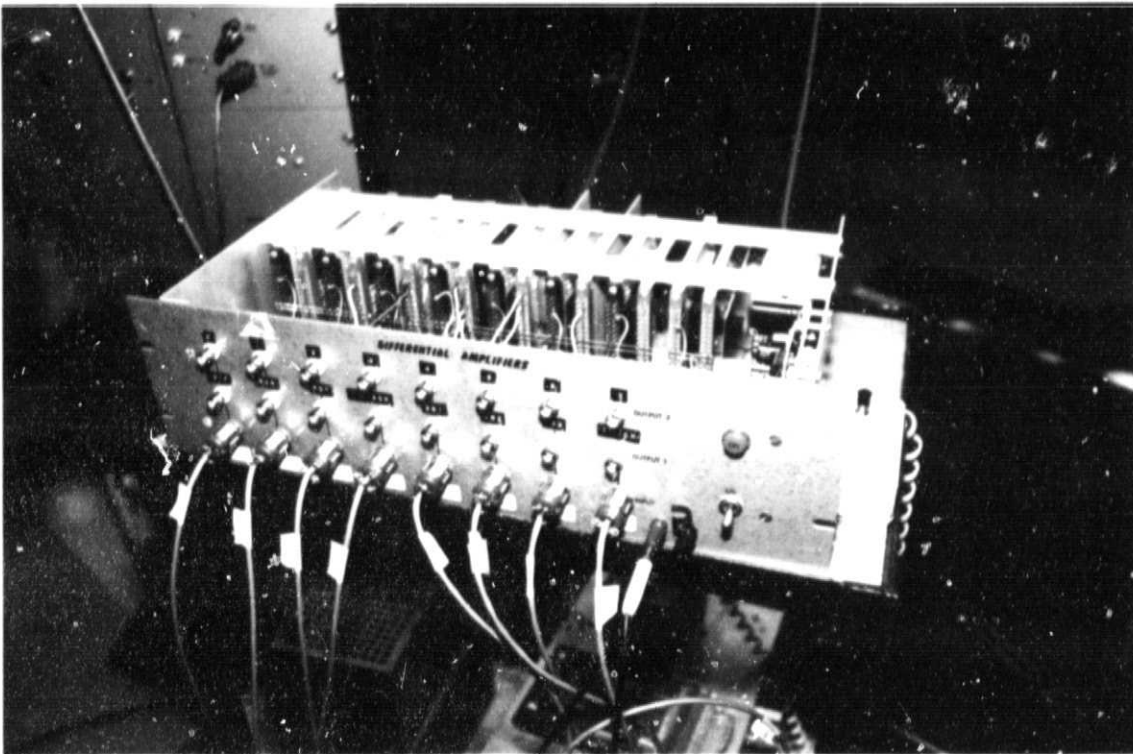


Fig. 2.6 Electronics rack :

it contains the differential amplifiers used for amplification and filtering of the sensors signals.

ORIGINAL PAGE
COLOR PHOTOGRAPH

2.1 Experimental set-up

The latest version of the one-meter-long experimental arm, shown in Figures 2.1 and 2.2, was designed by Gene Duval, mechanical designer. It is mounted on the shaft of an Aeroflex torque motor with motion confined in the horizontal plane. The arm is very flexible in bending (first cantilevered vibration frequency is 0.5 Hz) but stiff in the other directions. The linearity of the arm elastic motion has been improved by using a high-grade Aluminum (2024-T3) for each beam and hardened Beryllium copper for the flex joints (see Figure 2.5). The torsional rigidity was increased by having a larger separation between each beam and adding more bridges (8).

End-point position sensing is obtained by focusing the image of a light-bulb mounted at the tip of the arm on an analog x-y photodetector made by United Detector Technology. The detector, fixed in the laboratory, has a limited field of view of about ± 20 degrees. Other sensors available for feedback are a pseudo-rate sensor mounted on the actuator shaft and strain-gauges glued on the arm itself (see Figure 2.4).

The overall experimental set-up was upgraded to a professional level by Jim Maples, electrical engineer. In particular, the following improvements were made:

1. replacement of the Magtech D.C. motor by a brushless limited-angle D.C. motor made by Aeroflex. The casing for the motor was designed by Gad Shelef and fabricated in the Aero/Astro department machine shop (see Figure 2.3). The linear range of the motor is about ± 50 degrees. The main advantage of this actuator is its linearity with much smaller friction than for the Magtech D.C. motor.
2. design and fabrication of a special purpose electronics rack which contains all the necessary analog amplifiers and filters for sensors signal conditioning. It is shown in Figure 2.6. For each sensor output, there is an amplifier with adjustable gain and adjustable low-pass filter (model 2B31J by Analog Devices). The hub potentiometer output as well as the strain-gauges outputs are also processed through analog differentiators.
3. a new Analog to Digital board (DAS 1151 made by Analog Devices) replaces the board from Data Translation because the later generated unacceptable random noise.
4. software improvements on the DEC Minc 11 laboratory computer (LSI 1123): several routines callable from Fortran were added to the user friendly library of programs available to drive the A/D, D/A and interrupt clock (JXLIB written by Jim Maples). This includes a fast matrix multiplication routine written in assembly language. The operating system is RT11 V.04.

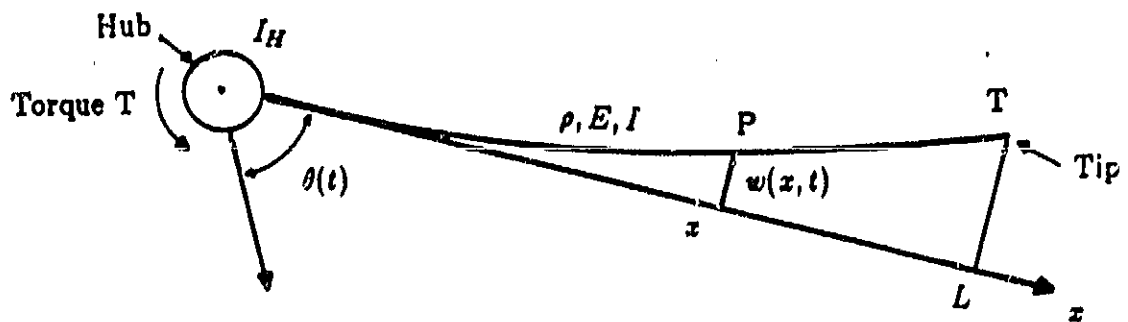


Fig. 2.7 Geometry of the arm model:
 the flexible arm neutral axis is shown together with the lumped hub inertia.

The computer codes used to implement the LQG and low-order compensators were re-written so that it is possible for the user to select a desired set of sensors as well as the order of the compensators.

Programs have been written by Jim Maples and Sandy Alexander to download automatically the control gains from the VAX computer to the MINC 11 so as to facilitate the design/experimental verification process.

5. software additions on the STAR-VAX 782 computer: a major improvement to our computational power was the installation of the computer-aided design program called CTRL-C made by Systems Control Technology. This package is based on the program "MATLAB", originally developed by C. Moler at the University of New Mexico. It is essentially a powerful "desk calculator" for multivariable linear control design (continuous and discrete), digital signal processing and identification. It is also a convenient laboratory tool for data manipulation and plotting. In particular, experimental data can be easily loaded in the program and then identification of the open-loop or closed-loop system can be performed by CTRL-C.

The user can write his (or her) own set of procedures which use the available primitives: new algorithms can be easily written with much faster turnaround development time than if they had to be programmed in Fortran.¹

2.2 Dynamic modelling

Figure 2.7 is a schematic of the arm neutral axis of length L . $\theta(t)$, the angle between a fixed reference and the tangent line at the root of the arm neutral axis, is measured with a film-wire potentiometer. The pseudo-rate is obtained by analog differentiation of $\theta(t)$. The tip sensor output is defined as

$$y_t(t) = w(L, t) + L\dot{\theta}(t) \quad (1)$$

where $w(x, t)$ is the elastic deflection measured from the tangent line at the root of the arm ($w(x, t)$ is assumed to be small). The output of a strain-gauge mounted at a distance x from the arm root, is proportional to the quantity $\frac{t_b}{2} \frac{d^2 w}{dx^2}(x, t)$, where t_b is the beam thickness.

The dynamic model is identified by open-loop sine sweep tests (see [1] for more details). The dynamic equations are given as a set of uncoupled second-order differential equations in modal form:

¹We believe that CTRL-C (like its competitor program Matrixx from Integrated Systems Incorporated) will become some sort of standard in universities as well as in control systems research and development centers.

ORIGINAL PAGE
OF POOR QUALITY

Mode no. i	Plant-free frequency F_i (Hz)	Modal damping ξ	Actuator modal gain $\frac{A_i}{L_i}$ (rad.)	Tip sensor modal gain $\phi(L)$ (m)	Strain-gauge modal gain $\frac{C_i}{L_i}$ (1/m)
0 (Rigid body)	0	0	1.5	1.12	0.0
1	1.98	0.015	2.97	-1.1	1.1
2	3.44	0.08	3.0	0.98	5.8
3	7.70	0.08	1.25	-1.21	11.72

TABLE 1 8th order model parameters for flexible arm with no payload

From this model, we can derive the open-loop s-plane transfer functions from torque input to a given sensor output (see appendix A).

3 Joint angle versus end-point position feedback

In this section, two simple control designs are developed, the first one using only *colocated position* sensor and actuator, the second one using the end-point position sensor *not colocated* with the actuator.

3.1 Conventional joint angle feedback

3.1.1 Design

Most of today's robot joint-angle controllers, either analog or digital, consist of a proportional, derivative and integral control network. The control parameters are designed for each joint, one at a time, either by analysis or perhaps more often by trial and error on a prototype.

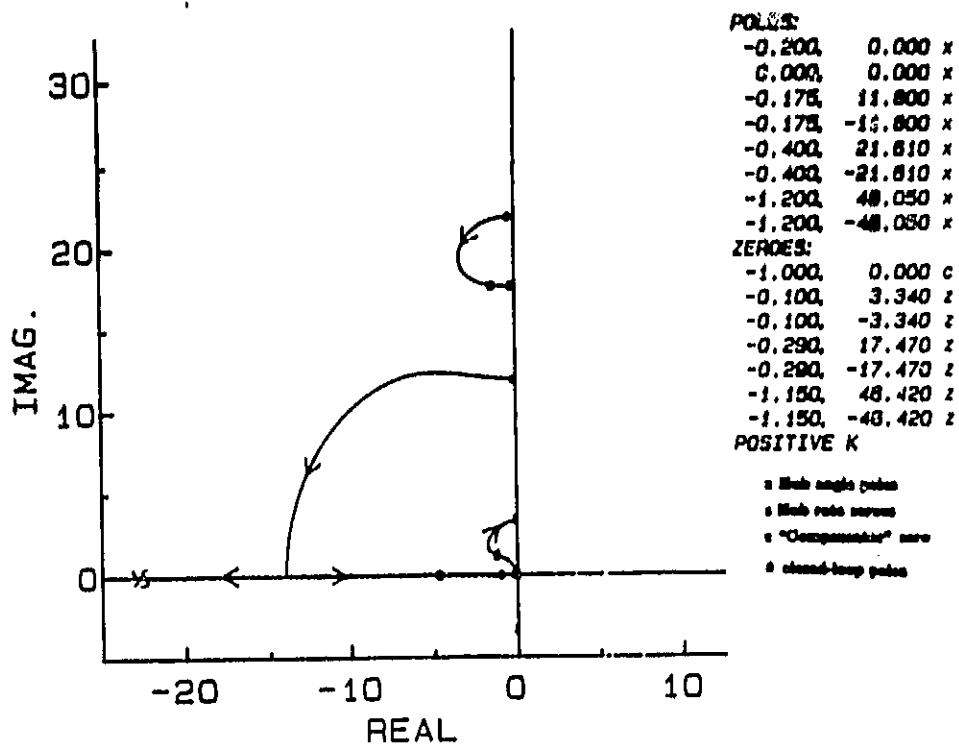


Fig. 3.1 Root-locus for proportional and derivative joint feedback: this locus is plotted versus the rate gain k_r .

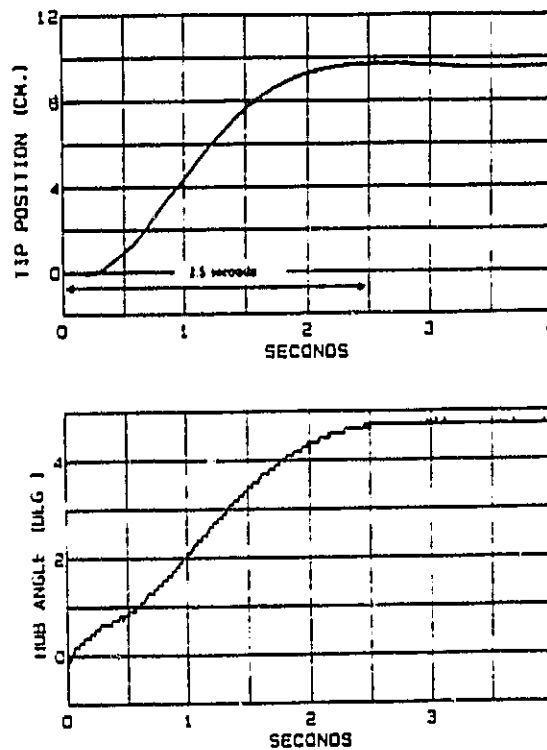


Fig. 3.2 Experimental step response: proportional and derivative joint feedback (low gain)

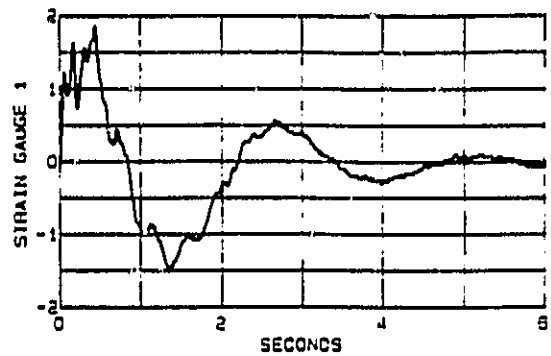
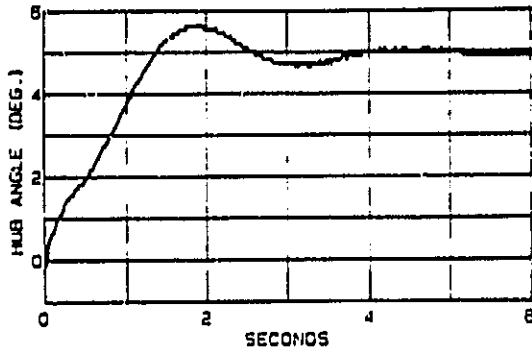
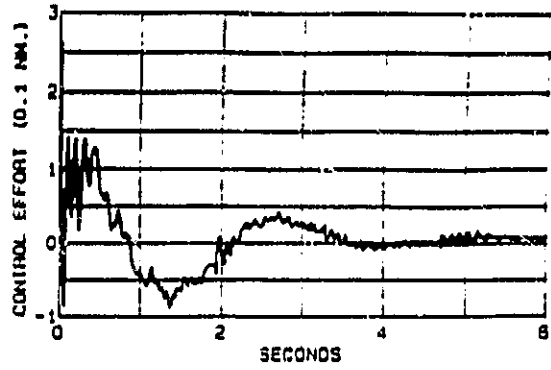
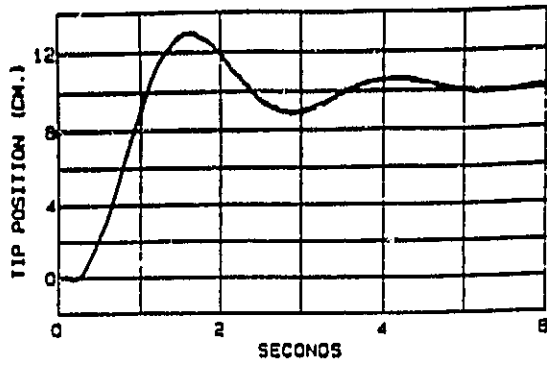


Fig. 3.3 Experimental step response:
 proportional and derivative joint feedback (medium gain)

ORIGINAL PAGE IS
 OF POOR QUALITY

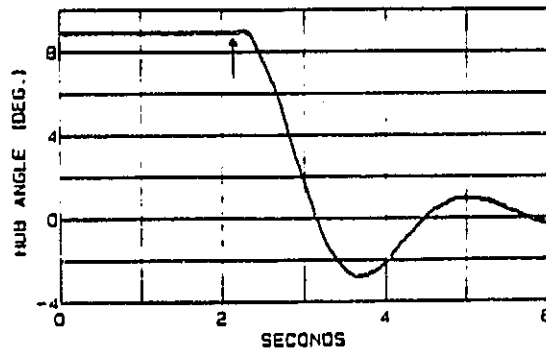
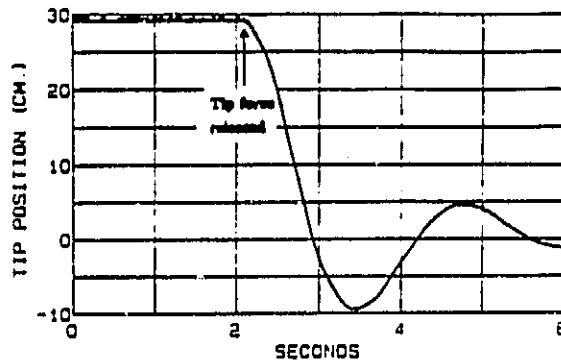


Fig. 3.4 Closed-loop response to a calibrated tip disturbance force release:
 same control law as in Figure 3.3.

For a simple proportional and derivative hub angle feedback, the control torque $u(s)$ is given by

$$\begin{aligned} u(s) &= -k_p\theta(s) - k_r\dot{\theta}(s) \\ &= -k_r\left(s + \frac{k_p}{k_r}\right)\theta(s) \end{aligned} \quad (4)$$

The shape of the root-locus of the closed-loop poles depends on the location of the compensator "zero", $s_0 = -\frac{k_p}{k_r}$. Figure 3.1 shows a typical root-locus of the closed-loop poles versus the gain k_r , for a ratio of $\frac{k_p}{k_r}$ equal to 1 second.¹

For increasing k_r , the rigid-body closed-loop poles move from the origin of the s -plane towards the cantilevered zeroes. The first pair of cantilevered zeroes at $f = 0.5$ Hz limits the control bandwidth. The rigid hub of the beam will appear to be clamped for very large gains. For a gain $k_r = 1$ Nm/Rad/Sec⁻¹, the damping coefficient of the rigid body poles is equal to 0.7. The corresponding position feedback gain k_p , which is equal to 1 Nm/Rad, is a low gain: the feedback torque will reach its saturation value of 1 Nm only for a large initial error of 60 degrees. Because this arm is very flexible - resulting in cantilevered zeroes being close to the origin and in a large separation between the first zero/pole pair of the hub angle transfer function - a large value for the position gain k_p must be traded-off versus an adequate damping coefficient for the rigid-body poles.

Theoretically, this colocated control law results in infinite gain margins and 90 degrees of phase margin. However, the gain margin will be always finite and the phase margin will be lower for any practical system, because there is always unmodelled actuator and sensor dynamics as well as delays for discrete implementations. Nevertheless, the practical stability margins remain very good.

3.1.2 Experimental results

Figure 3.2 shows the experimental step response for the colocated control law implemented with a sampling rate of 100 Hz. The hub angle command is computed so that the resulting tip sensor offset is 10 cm. The hub angle reaches its commanded position in 2.5 seconds. There is nearly no overshoot in the response, as predicted by the design.

Figure 3.3 shows a response for a higher position gain, $k_p = 3$ Nm/Rad, and a position to rate gain ratio of 2 sec⁻¹. The rise time is shorter at the expense of more overshoot and smaller damping.

The recordings of Figure 3.4 were obtained by applying a known tip force which is then released. The control gains are the same as for Figure 3.3. It takes more than 4 seconds for the tip motion to be completely damped out.

¹The root-locus is also plotted versus the position gain k_p , because the ratio $\frac{k_p}{k_r}$ is fixed

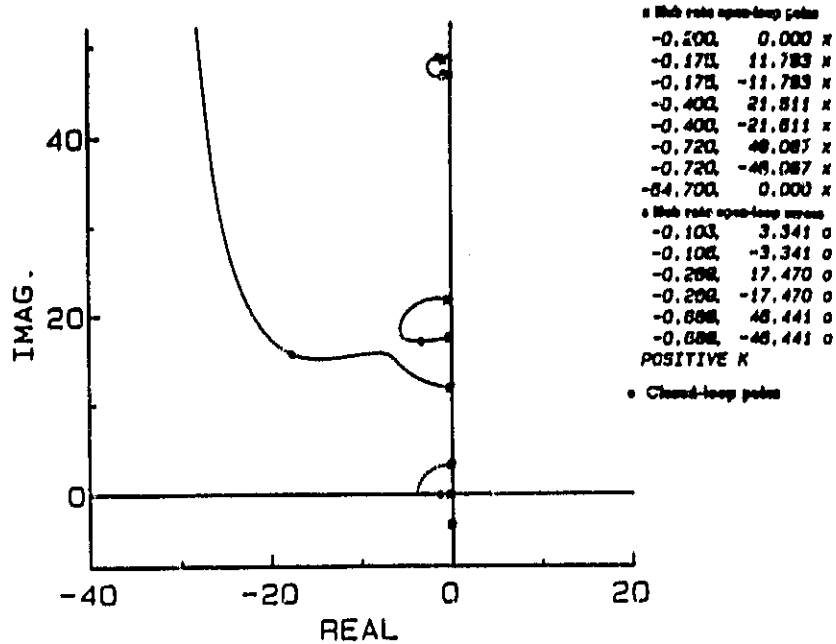


Fig. 3.5 (a) Root-locus for joint rate feedback

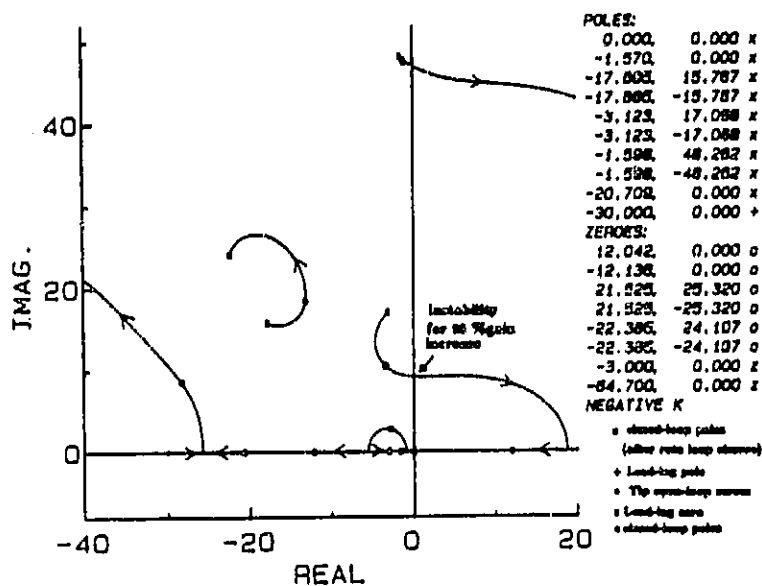


Fig. 3.5 (b) Root-locus for lead-lag tip position feedback: the joint rate loop is closed.

3.2 End-point feedback control

3.2.1 Design

If a proportional and derivative control law is used with the tip position sensor instead of the hub angle, the odd-numbered¹ flexible modes (#1 and #3) become unstable for an extremely low gain. A simple end-point controller consists of a combination of hub rate gain feedback and a lead-lag compensator for the tip sensor. The corresponding control torque $u(s)$ is expressed as

$$u(s) = -k_r \dot{\theta}(s) - k_{yt} \frac{\left(\frac{s}{a} + 1\right)}{\left(\frac{s}{b} + 1\right)} y_t(s) \quad (5)$$

In order to find adequate values for the four design parameters k_r , k_t , a and b in Equation (5), we use the method of successive loop closure:

- ▶ rate loop closure: a root-locus versus the gain k_r is shown in Figure 3.5.a This locus is slightly different from the one for the standard collocated rate feedback, because the rate sensor model includes a first-order pole at 10 Hz. Still the gain margin for the analog rate loop is large. k_r is chosen so that the damping coefficient of the first vibration mode is equal to about 0.7: $k_r = 0.5$ Nm/Rad/sec.
- ▶ tip loop closure: for $a = 3 \text{ sec}^{-1}$ and $b = 30 \text{ sec}^{-1}$, a root-locus of the closed-loop poles versus the gain k_{yt} is displayed in Figure 3.5.b The closed-loop rigid-body poles have a damping coefficient of 0.7 for a gain value of $k_{yt} = 3.0$ Nm/m. If the tip sensor gain is increased by 65 % from this design value, the closed-loop rigid body poles become unstable. This relatively low gain margin for the tip loop is explained by the attraction of the right-half plane zeroes. It is *characteristic* of a "strongly" non-minimum phase system.

Another interesting result is that because of the collocated rate feedback loop, the overall actuator loop transfer function $GK(s)$ has become "less" non-minimum-phase than if there were no rate feedback at all. More will be said on that subject in the section 4.4.3.

3.2.2 Experimental results

The control law is implemented with a sampling rate of 100 Hz. Experimental recordings of the sensor outputs are shown in Figure 3.6 together with simulated outputs for a position step command of 10 cm.

¹These modes, also called "unstably-interactive modes", whose modal gains $\phi_i(L)$ are of opposite signs to the hub modal gains $\frac{d\phi_i}{dx}(0)$.

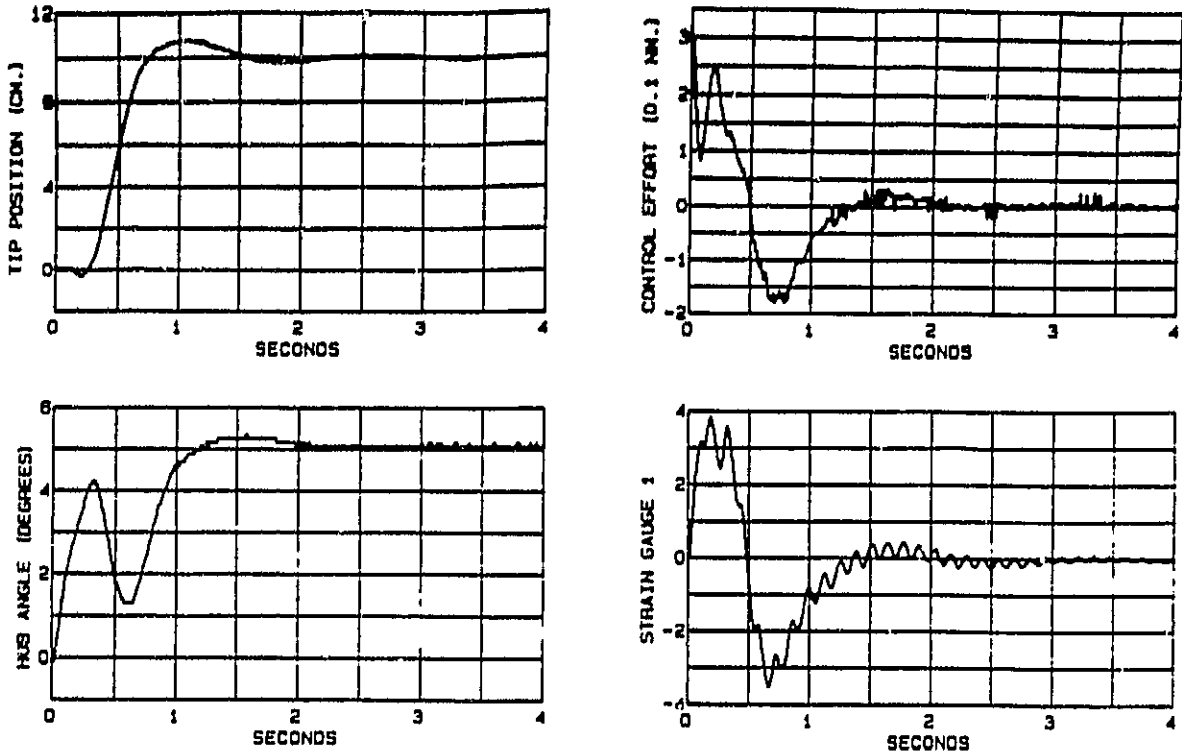


Fig. 3.6 (a) Experimental step response:
tip position lead-lag and joint rate feedback (medium gain)

tip lead-lag and hub rate gain

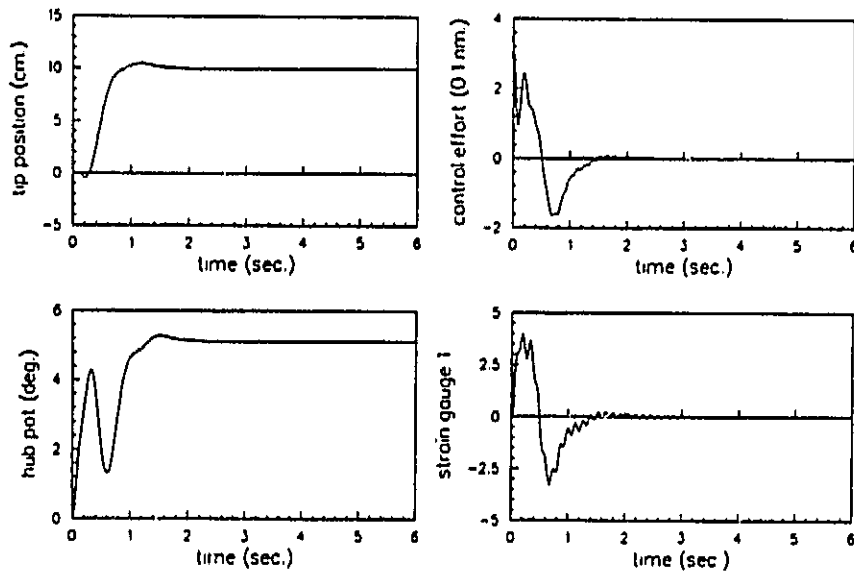


Fig. 3.6 (b) Simulated step response:
tip position lead-lag and joint rate feedback (medium gain)

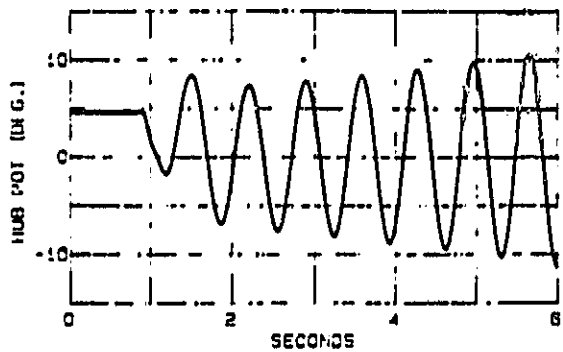
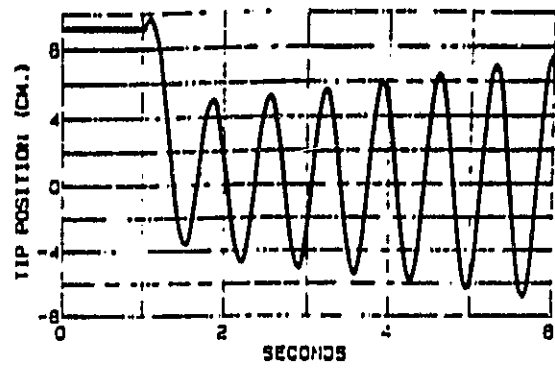


Fig. 3.7 Experimental step response:
tip position gain is increased by 70 % from its design value.

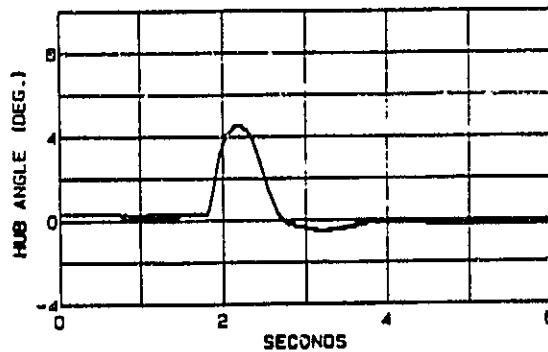
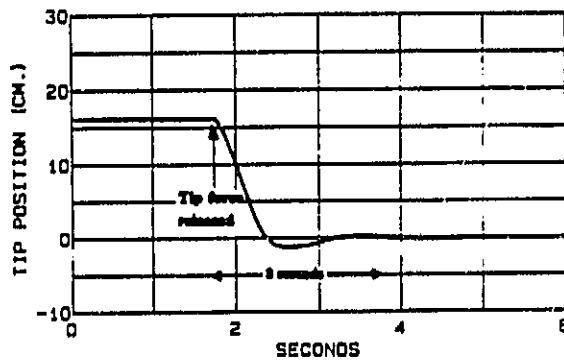


Fig. 3.8 Closed-loop response to a calibrated tip disturbance force release:
same control law as in Figure 3.6.

ORIGINAL PAGE IS
OF POOR QUALITY.

The key features of this step response are (1) a 130 msec. pure delay between initial command and first actual motion of the tip, (2) the non-minimum phase behavior of the tip motion and (3) the forward and reverse motion of the hub angle. This typical hub motion *is not produced* "naturally" for the case of the colocated control law (1) of the previous section. (Obviously, this is not true for the case of a high-order compensator - using hub angle feedback control only).

Notice the lightly damped small component at the third vibration mode frequency, which is present in the strain-gauge output. Agreement between experiment and simulation is quite good.

The recordings of Figure 3.7 shows the system response to initial conditions when the tip gain k_t is increased by 70 % from its nominal value. In agreement with the analysis, the control system becomes unstable. The frequency of the unstable mode ($f \simeq 1.45$ Hz) is the one predicted from the root-locus shown in Figure 3.2.

Finally, Figure 3.8 is the counterpart to Figure 3.4, showing the response of the nominal system to the same disturbance force release for the end-point position controller, yielding faster damped tip motion than for the colocated control (2 seconds instead of 4 seconds) . The disturbance response of a dynamic system is always improved at the location where sensing occurs.

4 LQG design and performance

The LQG modern control approach has the primary advantage of being able to handle multi-input multi-output systems [3]. In the last ten years, a considerable research effort has been devoted to the practical use of LQG control design techniques. The concepts of design constraints and stability margins previously developed for SISO systems have been extended to MIMO systems, [4], [5]. These results are directly applicable to our design problem. Although the experimental set-up involves only one actuator, it is still a truly multi-output system because in addition to the prime end-point sensor, we have used a colocated rate sensor and strain-gauges mounted on the beam. Attempts to design a tip control system with three sensors by the classical method of successive loop closures proved to be a rather difficult task. With the LQG approach, adding auxiliary sensors to a good nominal design is much simpler. Furthermore, once a satisfactory LQG design has been obtained for one flexible arm, it is easy to make a redesign for a different arm - for instance one that is 10 times stiffer.

The design of an LQG tip compensator was discussed in Reference 1. Using the separation theorem [3], regulator and estimator are designed independently.

After reviewing briefly the regulator design, we focus our discussion on the estimator and on the performance analysis results¹.

4.1 Regulator design

Because the quantity to be controlled is the tip position, y_t , the cost function J_r may be chosen as

$$J_r = \int_0^{\infty} \left(y_t^2 + r^2 \dot{y}_t^2 + \frac{u^2}{T_{max}^2} \right) dt \quad (6)$$

where an increase in weighting r adds more damping to the closed-loop regulator poles. T_{max} is a design parameter in units of Nm, and y_t is implicitly scaled in units of meters. The full-state feedback gains C are computed from an automated computer code (Optsys, [5]) which solves for the steady-state Ricatti equation derived for the cost function (6) with the linear dynamic model (3). For $T_{max}^2 = 10^3 \text{ Nm}^2/\text{m}^2$, for example, we find that we can achieve the following well-damped poles:

$$-6.1 \pm 2.7j, \quad -7.7 \pm 11.4j, \quad -6.5 \pm 23.8j, \quad -5.4 \pm 48.5j.$$

[1] and [2] explain the *fundamental limit* of the tip closed-loop system to follow a given tip command. This limit does not depend on which sensors are used for feedback, but only on the flexible arm dynamics characteristics via the non-minimum phase open-loop tip transfer function. Physically, it is explained by the time required for a bending wave to travel from the actuator to the tip.

4.2 Continuous estimator design

Before starting any design, the first question to answer is which sensors will be used as inputs to the estimator. Depending on *which* sensors are used, the resulting closed-loop performance will change *drastically*.

The primary sensor is the the tip position sensor, whose output is to be controlled. A colocated rate sensor is also available and is known to be a good means for adding damping to a flexible system. Therefore, it seems reasonable to consider this sensor as an additional input to the estimator. Then, we have at our disposal strain gauges; they directly sense the amount of bending of the arm without measuring any rigid body motion, and they should also be useful to enhance the quality of the state estimate \hat{x} .

¹see reference [1] and [2] for more details on this subject, including experimental verification.

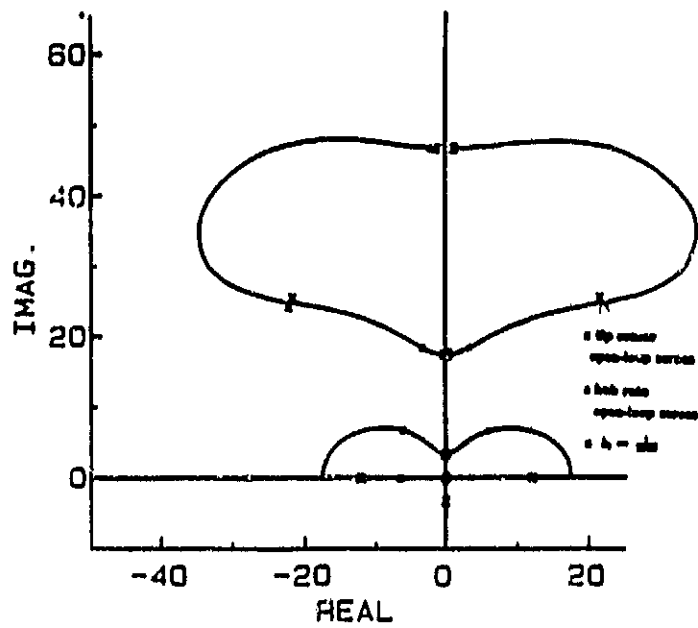


Fig. 4.1 Finite estimator poles root-locus:
 this locus is plotted versus the ratio of the tip sensor noise covariance to the hub rate sensor noise covariance.

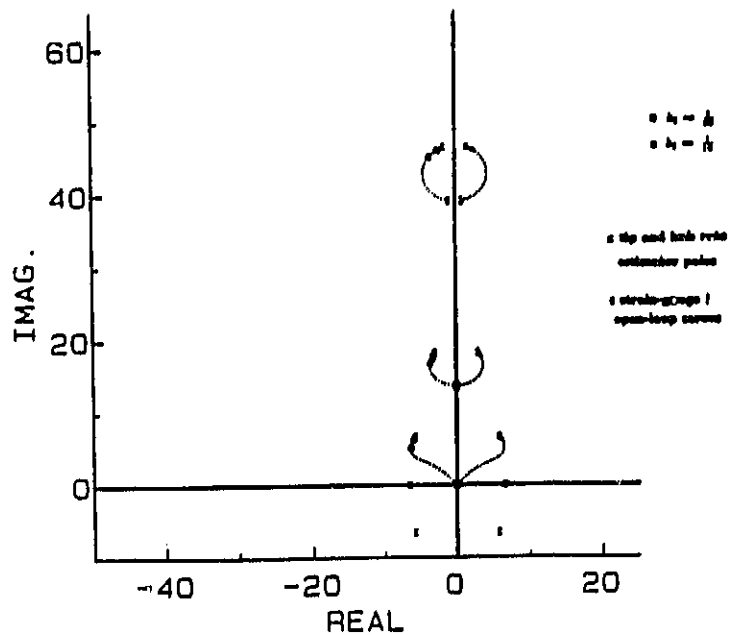


Fig. 4.2 Finite estimator poles root-locus:
 this locus is plotted versus the ratio of the tip sensor noise covariance to the strain gauge 1 sensor noise covariance.

We design several constant gain full-order state estimators. The three sensors considered as inputs to the estimator are the tip sensor, the colocated hub-rate sensor and the strain-gauge 1 (the closest to the hub). Estimator #1 uses the tip sensor only, Estimator #2 uses the tip and hub rate sensor and Estimator #3 uses tip, hub rate and strain-gauge 1 sensors. Our main design requirement is to obtain an estimator with fast and well damped closed-loop poles. Next, we discuss what is the relation between the noise covariance matrices and the closed-loop estimator pole locations.

The continuous steady-state LQG estimator reconstructs the "optimum" estimate \hat{x} of the state x for the following dynamic model :

$$\begin{aligned}\dot{x} &= Fx + \Gamma w \\ z &= Hx + v\end{aligned}\quad (7)$$

given w and v , random processes whose covariance matrices are respectively Q and R . R is a diagonal matrix with elements R_{v1} , $R_{\dot{\theta}}$, R_{ϵ_1} .

The LQG estimator design problem is then stated as follows:

- ▶ choose a process noise distribution vector Γ .
- ▶ choose adequate values for the covariance Q and for the ratios $k_1 = \frac{R_{v1}}{R_{\dot{\theta}}}$ and $k_2 = \frac{R_{v1}}{R_{\epsilon_1}}$.

The vector Γ is chosen equal to the actuator distribution vector G : therefore, we assume that the system is perturbed by a fictitious external actuator disturbance. As we will see later in section 4.4.2, this choice results in a closed-loop system with adequate disturbance rejection capabilities.

Following Doyle and Stein [5], this choice provides for adequate stability margins for the closed-loop system with respect to *actuator* gain and phase errors.

In order to choose the two ratios k_1 and k_2 , we know that the closed-loop estimator poles are the stable roots of the root square characteristic equation [3]:

$$\det\{R + Z(s)QZ^T(-s)\} = 0 \quad (8)$$

where $Z(s)$ is a column vector made of the three sensors open-loop transfer functions. When the ratio $\frac{Q}{R_{v1}}$ goes to infinity, six of the estimator poles will converge towards *finite* locations¹, while the remaining two poles converge to infinity in a second-order Butterworth pattern. As shown in Appendix B, we

¹These asymptotic poles are called "compromise zeroes" by Professor A.E. Bryson.

obtain the *asymptotic* locations of these finite estimator poles from Equation (8); they represent an upper limit on the maximum bandwidth attainable for an estimator driven by a given sensor set.

The results are the following:

- The finite estimator poles of Estimator 1 approach the stable open-loop tip transfer function zeroes, and the unstable zeroes reflected about the $j\omega$ axis: the slowest pair of poles will go to the location $s = -12$.

For $\frac{Q}{R_{v_i}} = 10^4 \text{ Nm}^2/\text{m}^2$, the estimator poles are:

$$-10.2 \pm 13.1j, \quad -8.9 \pm 2.9j, \quad -6.7 \pm 24.9j, \quad -3.5 \pm 48.5j.$$

- The finite poles of Estimator 2 belong to the stable part of a symmetric root locus versus the gain $k_1 = \frac{R_{v_i}}{R_j}$, as shown in Figure 4.1. These poles travel from the open-loop tip zeroes towards the open-loop hub rate zeroes (which are at the cantilevered frequencies). The choice of k_1 will dictate how much the hub rate sensor is used in the closed-loop system. As shown in the figure, adding the hub rate sensor decreases the maximum estimator bandwidth (but it has some prime advantages as we show in sections 4.4.2 and 4.4.3).

For $\frac{Q}{R_{v_i}} = 10^4 \text{ Nm}^2/\text{m}^2$ and $k_1 = 2000 \text{ m}^2/\text{Rad}/\text{Sec}^2$, the estimator poles are:

$$-6.6, \quad -99.4, \quad -5.9 \pm 6.6j, \quad -3.0 \pm 18.3j, \quad -1.7 \pm 46.7j.$$

- For each value of the ratio k_1 , the finite poles of Estimator 3 again belong to a locus versus the gain $k_2 = \frac{R_{v_i}}{R_{i_1}}$. One such locus is shown in Figure 4.2 for the previously chosen ratio $k_1 = 2000 \text{ m}^2/\text{Rad}/\text{Sec}^2$. Again, for increasing values of k_2 , one pair of estimator poles will move toward the origin: this indicates that for large k_2 , the rigid body information from the tip sensor is lost at the expense of the strain gauge signal. For $\frac{Q}{R_{v_i}} = 10^4 \text{ Nm}^2/\text{m}^2$ and $k_2 = \frac{1}{30} \text{ m}^2/\text{Rad}^2$, the estimator poles are:

$$-7.5, \quad -98.4, \quad -6.4 \pm 5.8j, \quad -3.5 \pm 17.6j, \quad -2.6 \pm 46.2j.$$

For $\frac{Q}{R_{v_i}} = 10^4 \text{ Nm}^2/\text{m}^2$ and $k_2 = \frac{1}{10} \text{ m}^2/\text{Rad}^2$, the estimator poles are:

$$-13.3, \quad -96.3, \quad -5.9 \pm 4.0j, \quad -3.7 \pm 16.4j, \quad -3.6 \pm 45.3j.$$

In conclusion, the method described above gives a guideline to choose the sensor noise covariance ratios k_1 and k_2 . The process noise covariance Q is increased iteratively until the finite estimator locations get close to their asymptotic locations discussed above. Once Q and R have been chosen, a computed code (Optsys, [6],[8]) is used to solve for the steady-state filter gains K .

This method could be extended to multi-input designs: for instance for a two-input system, there will be one more design ratio, the ratio of Actuator 2 process noise covariance over the one of Actuator 1. This ratio balances the participation of one actuator versus the other.

4.3 Closed-loop performance

The combined continuous regulator/estimator can be viewed as a classical compensator whose transfer function is: $H(s) = -C(sI - F + GC + KH)^{-1}Ky(s)$ where the transfer function matrix $H(s)$ is a row matrix with up to three elements, C is a row matrix for the full-state feedback gains, and K is the filter gain matrix with up to 3 columns. From the previous section, we obtain three different feedback systems which originate from the same regulator design but from different estimators: Compensator #1 uses only the tip position for feedback; Compensator #2 uses the hub rate in addition; Compensator #3 uses both hub rate and strain gauge 1 in addition. Table 2 summarizes the design parameters chosen for these three compensators. Our objective is to compare their closed-loop performance.

All the results discussed in this section have been obtained for the s-plane design, unless mentioned otherwise. The discrete implementation is discussed in Appendix D, following the approach of Katz and Powell [8].

noise covariance	Q (Nm ²)	$R_{\dot{y}}$ (m ²)	$R_{\dot{y}}$ (Rd ² /sec. ²)	R_{ϵ} (Rd. ²)
tip only	10 ⁴	1	∞	∞
tip and hub rate	10 ⁴	1	2000	∞
tip, hub rate and strain gauge	10 ⁴	1	2000	30

TABLE 2 s-plane weighting matrices used for the three different compensators:

4.3.1 Step response command

The standard way to implement a tip command y_{tc} to the LQG compensator is to feed the command to both the actuator and the estimator.

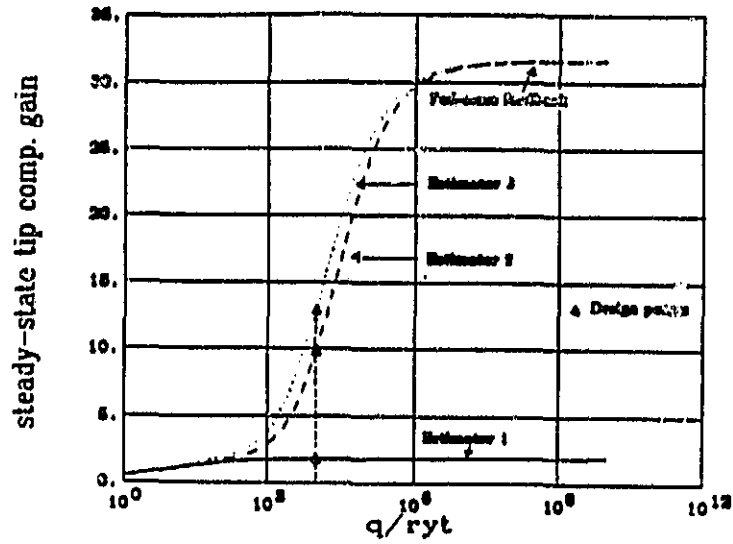


Fig. 4.3 Tip compensator steady-state gain:
 the gain is plotted versus the design ratio of the actuator noise to the tip sensor noise intensity; this is done for three different compensators.

The resulting equations are :

$$\begin{aligned}\dot{\hat{x}} &= (F - GC - KH)\hat{x} + Gu_c + Ky \\ u &= -C\hat{x} + u_c \\ u_c &= K_{ref}y_{tc}\end{aligned}\tag{9}$$

K_{ref} is chosen so that the steady-state gain from commanded to actual tip position is unity. As long as the actual beam dynamics does not deviate from the model, and the estimator is not excited by unmodelled external disturbances, we know by the separation theorem that the closed-loop transfer function from tip command to tip position will be given by:

$$\frac{y_t(s)}{y_{tc}(s)} = \frac{N_{ol}(s)}{\det(sI - F + GC)}\tag{10}$$

where $N_{ol}(s)$ is the zeroes of the open-loop tip numerator. Consequently, whether the hub rate and/or the strain-gauge are fed back or not in addition to the tip position measurement, the tip step response will be the same. Furthermore, even if the hub angle is used for feedback instead of the tip position, Equation (10) still holds.

4.3.2 Disturbance response

One of the most important items to consider when designing a robot positioning system is the effect of actuator friction. If T_d is the average friction from the D.C. motor, the resulting offset error on the tip position will be: $y_e = \frac{T_d}{K_{ss}}$, where K_{ss} is the steady-state tip compensator gain. Therefore the design goal is to make K_{ss} as large as possible.

The expression for K_{ss} is given by : $K_{ss} = -C(-F + GC + KH)^{-1}K_t$ where K_t is the tip filter gain. Figure 4.3 shows a plot of K_{ss} as a function of the design ratio $\frac{Q}{R_{vt}}$, for the three different compensators. We first notice the dramatic improvement when the hub rate is added in the feedback system. The limitation in K_{ss} for a "tip only" compensator is due to the non-minimum phase properties of the open-loop tip transfer function. When the hub rate is added, K_{ss} will tend asymptotically toward the asymptotic value it would have for full-state feedback; this value depends only on the regulator gains; it does not depend on the estimator gains as long as the system (F, G, H_z) - where H_z is the measurement vector- has no non-minimum phase transmission zeroes. When the nearly-cocated strain-gauge is added to the estimator, the rate of convergence of K_{ss} toward its asymptotic value is faster than for the "tip and hub rate" compensator as shown in Figure 4.3.

4.3.3 Robustness

In the design of a feedback control system, the most important step is to assess how much error can be tolerated in the system parameters before instability occurs. In the present section, we study two types of parameter errors:

1. variation in the open-loop frequencies.
2. gain and phase errors in the actuator loop and in the tip sensor loop.

Sensitivity to open-loop vibration frequencies:

For the three compensators designed previously, each vibration frequency (i.e. one eigenvalue of F) is increased or decreased by a given step, one at a time; the closed-loop eigenvalues of the total feedback system are computed at each step, until a pair of closed-loop eigenvalues goes in the right-half plane. The results are summarized in Table 3. The "tip only" compensator is very sensitive to the open-loop vibration mode frequencies, because it relies on highly tuned notch filters to provide damping to the system. As soon as the hub rate is added in the feedback loop, the closed-loop system becomes less sensitive. There is further improvement when the strain gauge 1 is also added.

compensator #	1	2	3
% increase modal frequency 1	25	40	87
% decrease modal frequency 1	16	45	100
% increase modal frequency 2	72	26	>100
% decrease modal frequency 2	26	25	32
% increase modal frequency 3	>100	>100	>100
% decrease modal frequency 3	27	29	56

TABLE 3 Allowable error in the open-loop vibration frequencies:
instability will occur for the percentage error indicated

Stability margins

Actuator loop:

For a single-input single-output system, the stability margins with respect to actuator dynamics are obtained by studying a Bode plot of the open-loop transfer function " $G(s)K(s)$ ", where $G(s)$ and $K(s)$ are respectively the open-loop model and the compensator transfer function.

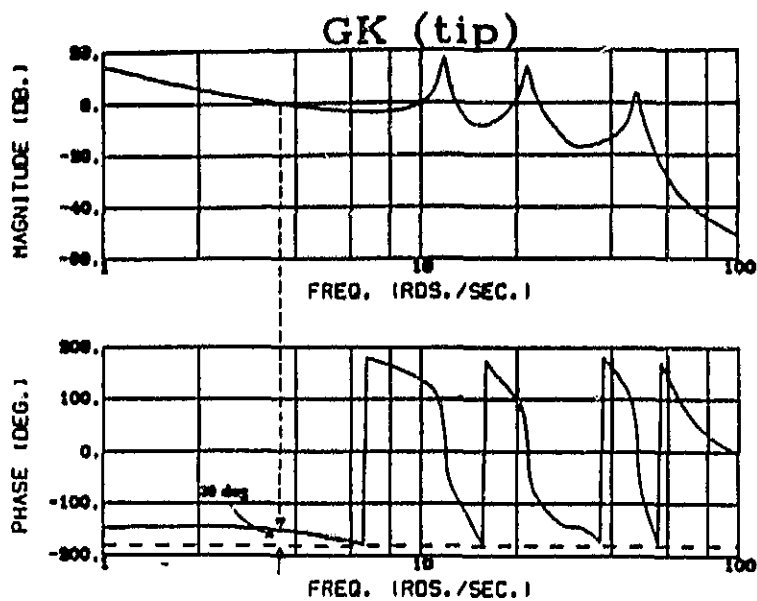


Fig. 4.4 Bode plot of open-loop transfer function $GK(s)$:
only the tip sensor is feedback

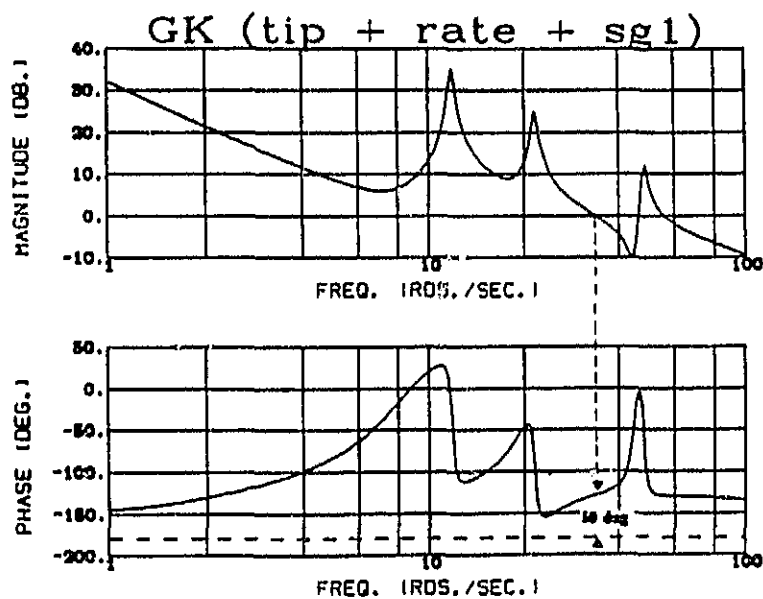


Fig. 4.5 Bode plot of open-loop transfer function $GK(s)$:
the tip, hub rate and strain-gauge 1 sensors are feedback.

For a single-input multi-output system, it is also possible to compute the open-loop transfer function $GK(s)$ as shown in Appendix C. Figures 4.4 and 4.5 are the Bode plots of $GK(s)$ respectively for the "tip only" (#1) and for the "tip, hub rate and strain gauge 1" (#3) compensators. For Compensator #1, the rigid body gain margin is 3 dB at $\omega_c = 4$ Rad/sec and the phase margin, 30 degrees. For Compensator #3, the phase always stays above -180 degrees. There is theoretically no gain margin limit; in reality, there will always be a finite gain margin because of unmodelled phase lags that occur at higher frequencies. The crossover frequency is much higher, $\omega_c = 35$ rad/sec. The phase margin is about 50 degrees, a noticeable improvement compared to Compensator #1. Compensator #3 corresponds to a high gain system.

Its transfer function $GK(s)$ has become minimum phase, while it was non-minimum phase for Compensator #1. The main advantage provided by a minimum-phase $GK(s)$ is less sensitivity to actuator gain increase. The same thing happens for Compensator #2. It seems that with high gain colocated rate feedback, the open-loop transfer function $GK(s)$ becomes minimum-phase again. The generalization of this statement to an arbitrary elastic structure is left for future research.

Doyle and Stein [4] [5] have shown that by increasing the actuator process noise in the estimator design, the open-loop transfer function $GK(s)$ tends asymptotically towards the full-state feedback transfer function. This enables the closed-loop system to "recover" the stability margins of the full-state feedback regulator obtained for the actuator loop (60 degrees of phase margin and at least 6 dB of gain margin). One necessary condition is that the open-loop system transfer function be minimum-phase.

The only concern in examining the gain plot of Figure 4.5 is the crossover frequency at 35 rad/sec, which might be too high. At the same time, it might also be useful to increase the roll-off at high frequencies from $\frac{1}{s}$ to $\frac{1}{s^2}$. These two improvements could be obtained by adding an actuator low-pass filter in the regulator design, or by making the process noise colored instead of white in the estimator design.

Tip sensor loop:

Because our primary goal is to control the tip position, it is also necessary to study the stability margins of the tip sensor loop, with all the other feedback loops closed. The corresponding transfer function $G_{y_t}K_{y_t}(s)$ is derived in Appendix C. For the "tip only" compensator, the transfer function $G_{y_t}K_{y_t}(s)$ is the same as the actuator transfer function, $GK(s)$, and the corresponding margins are given above. For Compensator #3, the rigid body gain margin is about 3.7 dB, which corresponds to a tip gain increase of 55%. This relatively small gain margin seems to be characteristic of the non-minimum-phase open-loop tip transfer function. In order to get good performance for the tip position loop,

either we have to rely on an accurate model of the system, or we have to identify the model on-line, a first step toward adaptation. The rigid-body phase margin is about 35 degrees (which is acceptable).

5 Low-order compensator

One drawback of the LQG compensators described in the previous section is that they might be unnecessarily complicated. This is especially true for designing a position controller for a multi-link elastic robot with linearized dynamics. Low-order compensators might provide for similar performance while being simpler to implement.

5.1 Description of the design algorithm

An output feedback control design algorithm for the design of low-order controllers is described [9]. Given a linear dynamic system

$$\begin{aligned}\dot{x} &= Fx + Gu + \Gamma w \\ y &= Hx + v\end{aligned}\tag{11}$$

where w and v are white noise processes, and assuming a feedback compensator in a minimal realization form

$$\begin{aligned}\dot{z} &= Az + By \\ u &= Cz + Dy\end{aligned}\tag{12}$$

the algorithm will find the elements of A , B , C and D ¹ by minimizing the standard LQG quadratic performance index,² J

$$J = \int_0^{\infty} e^{2\alpha t} (x^T Q_r x + u^T R_r u) dt\tag{13}$$

¹a non-zero column of the direct transmission matrix D requires the corresponding sensor to be either noise-free or contaminated by colored noise only

²The performance index J can also be chosen as a weighted sum of individual indexes for a set of different F , G , Γ and H matrices, so that the resulting design is robust to changes in the system parameters.

Instead of minimizing directly the steady-state performance index J , the optimization is done on a finite-time performance index J_t . Therefore the closed-loop system does not need to be stable initially and at each step of the optimization. Steady-state convergence is obtained by increasing t_f gradually. Note that the computational effort required by such an algorithm is still several orders of magnitudes higher than for the standard LQG design. The main difficulty for the user is to choose a proper compensator structure to be optimized. Although the initial guess for the compensator matrices A , B , C and D does not need to produce a stable closed-loop system, a "reasonable" initial guess will maximize the likelihood of a successful convergence as well as a "reasonable" optimized compensator.

5.2 Design procedure

We discuss in this section low-order compensators using the tip and the hub rate sensors. The weighting matrices and noise covariances are chosen the same as the ones previously obtained for the 8th order LQG compensators successfully tested. The LQG compensators provide for notch filters for the second and third vibration modes. After having set the 8th order compensator in a minimal realization form, the states associated with the third vibration mode are deleted. The resulting 6th order compensator is re-optimized with "Sandy". The same thing is done for the states of the second vibration mode notch filter. A 4th order compensator is finally obtained for the 8th order dynamic model. It is then optimized again for the 9th order model which includes the first-order low-pass filter of the pseudo-rate sensor.

In the course of this design process, the rigid-body closed-loop poles always remain too close to the origin resulting in a bandwidth of 0.5 Hz. Also, the damping coefficient of the first flexible mode tends to remain relatively small i.e., $\zeta = 0.2$. One remedy to this problem is to use a non-zero value for the destabilization factor α in Equation (13) so that the closed-loop poles have real parts less than $-\alpha$. The value of α is progressively increased from 0 to 3.0 sec^{-1} . One potential drawback of this method is that damping for the high frequency modes (the third vibration mode in particular) is artificially added, while it might be preferable not to do so.

5.3 Design #1

For all the compensators given in this section, the following units are used: Nm. for the control effort, meters for the tip sensor and Rad/sec for the hub rate sensor. The initial 8th order LQG Compensator #2 is transformed in a minimal realization form expressed as follows

$$A = \begin{pmatrix} 0 & 1 & 0 & 0 & 0 & 0 & 0 & 0 \\ -127.06 & -14.09 & 0 & 0 & 0 & 0 & 0 & 0 \\ 0 & 0 & -9.04 & 0 & 0 & 0 & 0 & 0 \\ 0 & 0 & 0 & -143.1 & 0 & 0 & 0 & 0 \\ 0 & 0 & 0 & 0 & 0 & 1 & 0 & 0 \\ 0 & 0 & 0 & 0 & -334.6 & -5.24 & 0 & 0 \\ 0 & 0 & 0 & 0 & 0 & 0 & 0 & 1 \\ 0 & 0 & 0 & 0 & 0 & 0 & -2212.9 & -3.87 \end{pmatrix} \quad (14)$$

$$B = \begin{pmatrix} 126.2 & -2.478 \\ 409.9 & 10.599 \\ 1235.9 & 6.53 \\ 646.18 & 101.82 \\ 4.68 & 0.136 \\ -305.16 & -9.39 \\ 0.395 & 0.01 \\ -108.16 & 4.0 \end{pmatrix} \quad (15)$$

$$C = (0 \quad -1 \quad -1 \quad -1 \quad 0 \quad -1 \quad 0 \quad -1) \quad (16)$$

As a result of the lengthy process discussed in the previous section, the following 4th order compensator is obtained

$$A = \begin{pmatrix} 0 & 1 & 0 & 0 \\ -90.66 & -12.4 & 0 & 0 \\ 0 & 0 & -12.04 & 0 \\ 0 & 0 & 0 & -193.0 \end{pmatrix} \quad (17)$$

$$B = \begin{pmatrix} 102.5 & -1.88 \\ -362.0 & 11.0 \\ 1362.7 & 0.0 \\ 0.0 & 153.10 \end{pmatrix} \quad (18)$$

$$C = (0 \quad -1 \quad -1 \quad -1) \quad (19)$$

The closed-loop poles for this feedback law are all well damped (with real part less than -4 sec^{-1}) and about as fast as the one of the LQG design. Also the steady-state tip compensator gain is close to the LQG one (7.7 compare to 9.9 Nm/m). However, the phase margin of the actuator loop $GK(s)$ is only 20 degrees at 6 Hz. If a discretized version of this compensator were implemented with a 50 Hz. sampling rate, the resulting closed-loop system would be unstable. The reason is that the phase lag caused by a 50 Hz. sampling and zero-order-hold process is about 22 degrees at 6 Hz.

($\Phi \simeq 57.3 \omega \frac{T_s}{2}$ degrees, where T_s is the sampling period in seconds and ω is the frequency of interest in Rad/sec).

In the next section, we discuss one method to improve the phase margin of the actuator loop $GK(s)$.

5.4 Design #2

An approximate model for the phase lag caused by the sampling and zero-order-hold process is added to the dynamic model. The corresponding transfer function $H(s)$ for a delay of $\frac{T_s}{2}$ seconds (or equivalently a sampling rate of $2f_o$ Hz.) is

$$H(s) = \frac{(\frac{-s}{4f_o} + 1)}{(\frac{s}{4f_o} + 1)} \quad (20)$$

The augmented dynamic equations become

$$F_{aug} = \begin{pmatrix} F & G \\ 0 & -4f_o \end{pmatrix} \quad G_{aug} = \begin{pmatrix} -G \\ 8f_o \end{pmatrix} \quad (21)$$

The sampling rate f_o is chosen equal to 50 Hz. The 4th order compensator of Design #1 is the initial guess with the augmented 10th order system. The new optimization by "Sandy" yields the following compensator:

$$A = \begin{pmatrix} 0 & 1 & 0 & 0 \\ -155.56 & -21.73 & 0 & 0 \\ 0 & 0 & -10.2 & 0 \\ 0 & 0 & 0 & -607.5 \end{pmatrix} \quad (22)$$

$$B = \begin{pmatrix} 193.7 & -0.95 \\ -1021.7 & 3.56 \\ 2030.4 & 0.0 \\ 0.0 & 546.7 \end{pmatrix} \quad (23)$$

$$C = (0 \quad -1 \quad -1 \quad -1) \quad (24)$$

The phase margin of the original dynamic system for the actuator loop transfer function $GK(s)$ is now 40 degrees. The artificial phase lag of 20 degrees at 6 Hz. is essentially recovered. The closed-loop eigenvalues compare favorably with the ones for Design #1. However, the tip compensator D.C. gain is lower (5.6 Nm/m), because some performance must be traded-off versus stability margins.

5.5 Experimental verification

5.5.1 Implementation

The continuous compensator equations (12) are discretized via a zero-order-hold.

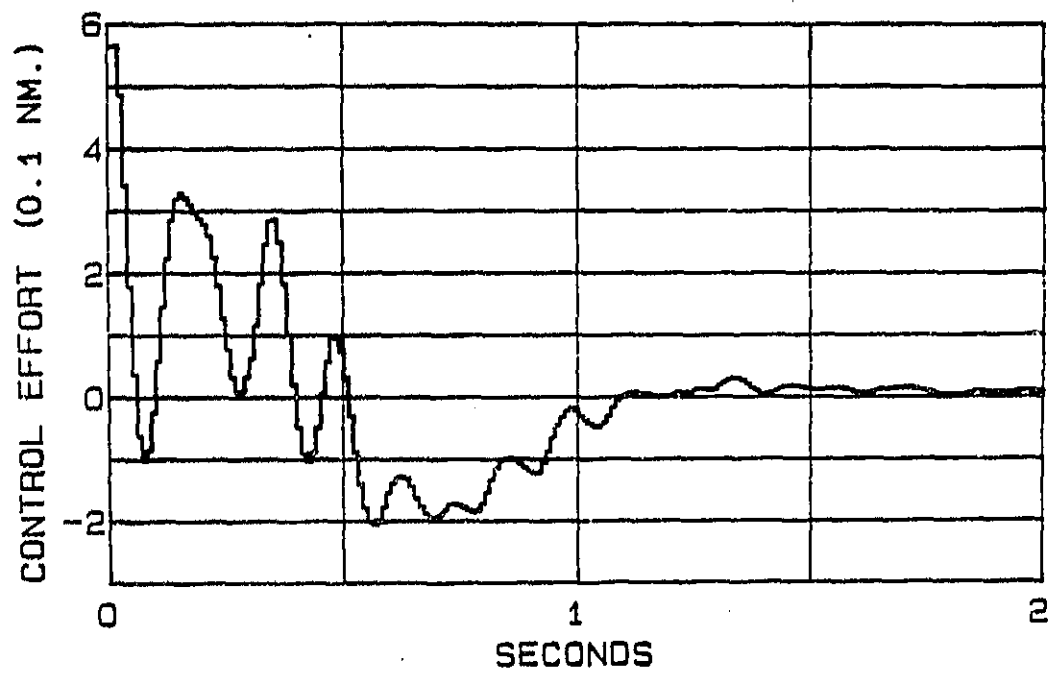
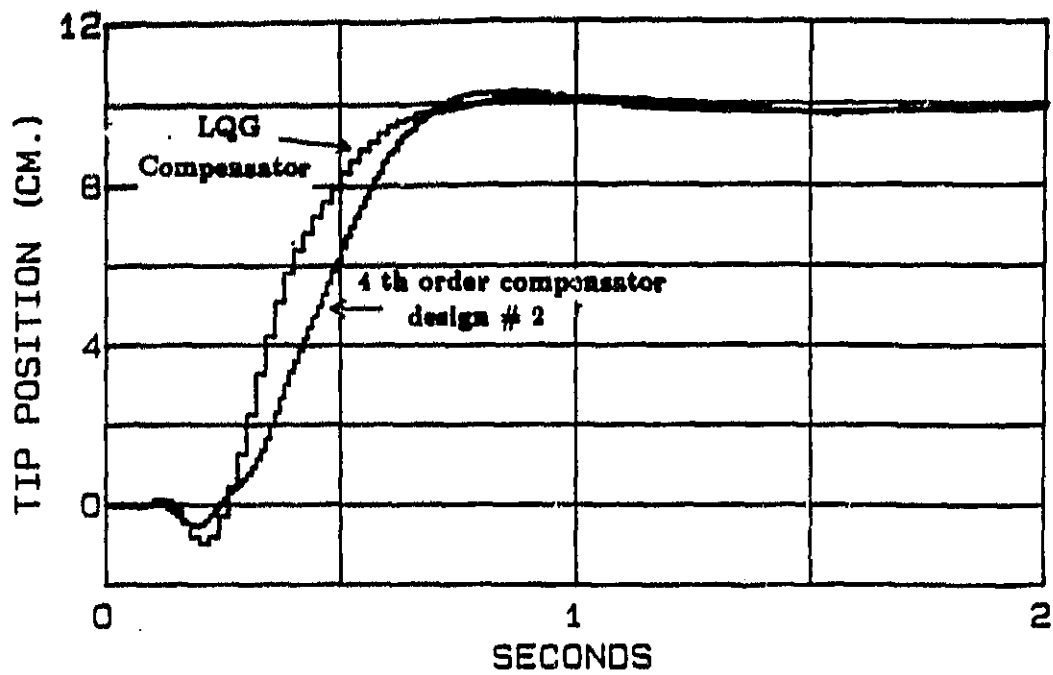


Fig. 5.1 Response of the tip-sensor-controlled flexible arm to a step command with the 4th order compensator #2.

To improve the phase matching between the continuous and the discrete compensator, a "current" version of the compensator is used

$$\begin{aligned} z(k+1) &= A_d z(k) + B_d \frac{(2y(k+1) + y(k))}{3.0} \\ u(k) &= C z(k) \end{aligned} \quad (25)$$

This is equivalent to adding a discrete compensator zero at $z = -0.5$. A_d and B_d are the discretized version of A and B for a zero-order-hold process. The resulting compensator is then recast in a form with a direct transmission term.

5.5.2 Closed-loop response

A step response for a 10 cm command is shown in Figure 5.1 for Design #2. The trace corresponding to the LQG design is shown superimposed. The low-order compensator compares favorably with the LQG full-order compensator.

The main drawback of this low-order design method is that it is not yet available as a direct discrete design method, therefore requiring fast sampling rates¹. Also, design by this method is really computationally intensive, and further improvements are needed in the algorithm implementation (1) to obtain faster convergence (2) to add "safeguard" limits in the optimization process where for example the compensator poles and zeroes are constrained to stay in a given region of the s-plane. Also, it would be useful for the user to have some graphics display in order to monitor the optimization process and therefore to have more control on it.

Nevertheless, this computer code is very attractive because it allows the designer to specify general compensator structures. Its application should be well-suited for the compensator design for linearized version of a multi-link elastic manipulator.

6 Switching between sensor sets

6.1 Motivation

Perhaps the most immediate robotics application of end-point position feedback is for accurate pick and place operations.

¹As mentioned previously, it might be possible to alleviate part of this problem by adding more roll-off in the actuator loop transfer function. It is not clear at this point if this would imply some reduction in performance.

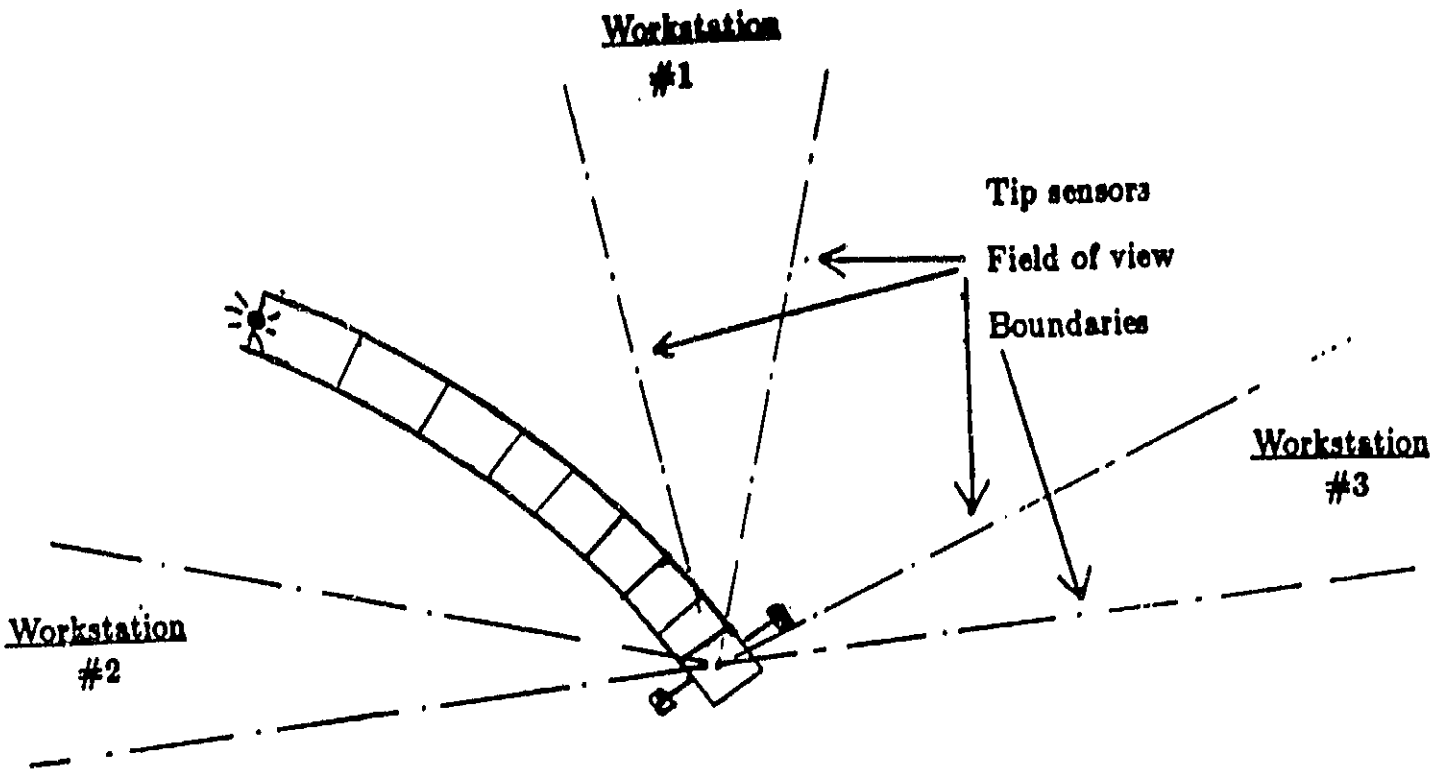


Fig. 6.1 Pick and place with several workstations.

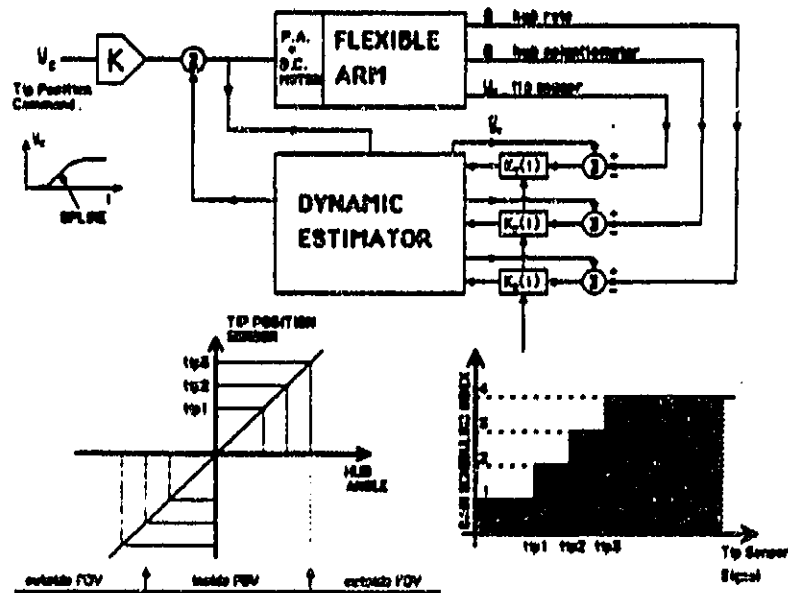


Fig. 6.2 Schematic of the control system with switching

ORIGINAL PAGE IS
OF POOR QUALITY

One can envision a series of workstations placed at several locations of the robot workspace, each being equipped with its own end-point sensor (see Figure 6.1). Because each tip sensor has a limited field of view, it becomes necessary to implement two different control modes:

- ▶ collocated mode: when the manipulator is outside a given tip sensor field of view, the only available position informations are from the joint angle sensors, which are therefore the primary sensors.
- ▶ non-collocated mode: once the manipulator is inside the tip sensor field of view, the end-point sensor is now the prime position sensor. Whenever the tip crosses in or out the boundaries of a given tip sensor field of view, switching must be implemented between these two control modes in such a way that no unwanted transients in the actuator(s) commands occur.

6.2 Proposed solution

When switching occurs between control modes, the arm dynamics does not change, only the available position sensors do. Consequently, if we stay in the frame of the LQG modern control theory (section 4), one possible solution is to implement a dynamic estimator whose gains will be varied as a function of the arm position. The tip sensor or the hub sensor are "faded" in or out depending on the actual location of the tip. This estimator reconstructs the *unique* beam dynamic state vector \hat{x} , which is then feedback to the actuator through a *unique* set of constant regulator gains.

6.3 Design of the estimator

In principle, the estimator discussed above is an estimator with time-varying gains, which could be computed by solving for the time-varying Ricatti equation where the tip and hub sensor noise covariances are made time-varying [10]. Outside the tip sensor field of view, the tip noise covariance is chosen very large compared to the hub sensor noise covariance: this makes the tip filter gains essentially equal to zero. Inside the tip sensor field of view, the situation is reversed.

For a practical implementation, a discrete set of constant estimator gains using the tip, hub angle and hub rate sensors is used. Somewhat arbitrarily, we chose to implement four sets of estimator gains: one set for outside the field of view for the hub position only (#1), two intermediate sets where both tip and hub sensor are used in the transition region of the tip sensor field of view (#2 and #3) and finally one set inside the field of view where the tip sensor only is used (#4). Figure 6.2 shows a block diagram of the corresponding control system implementation.

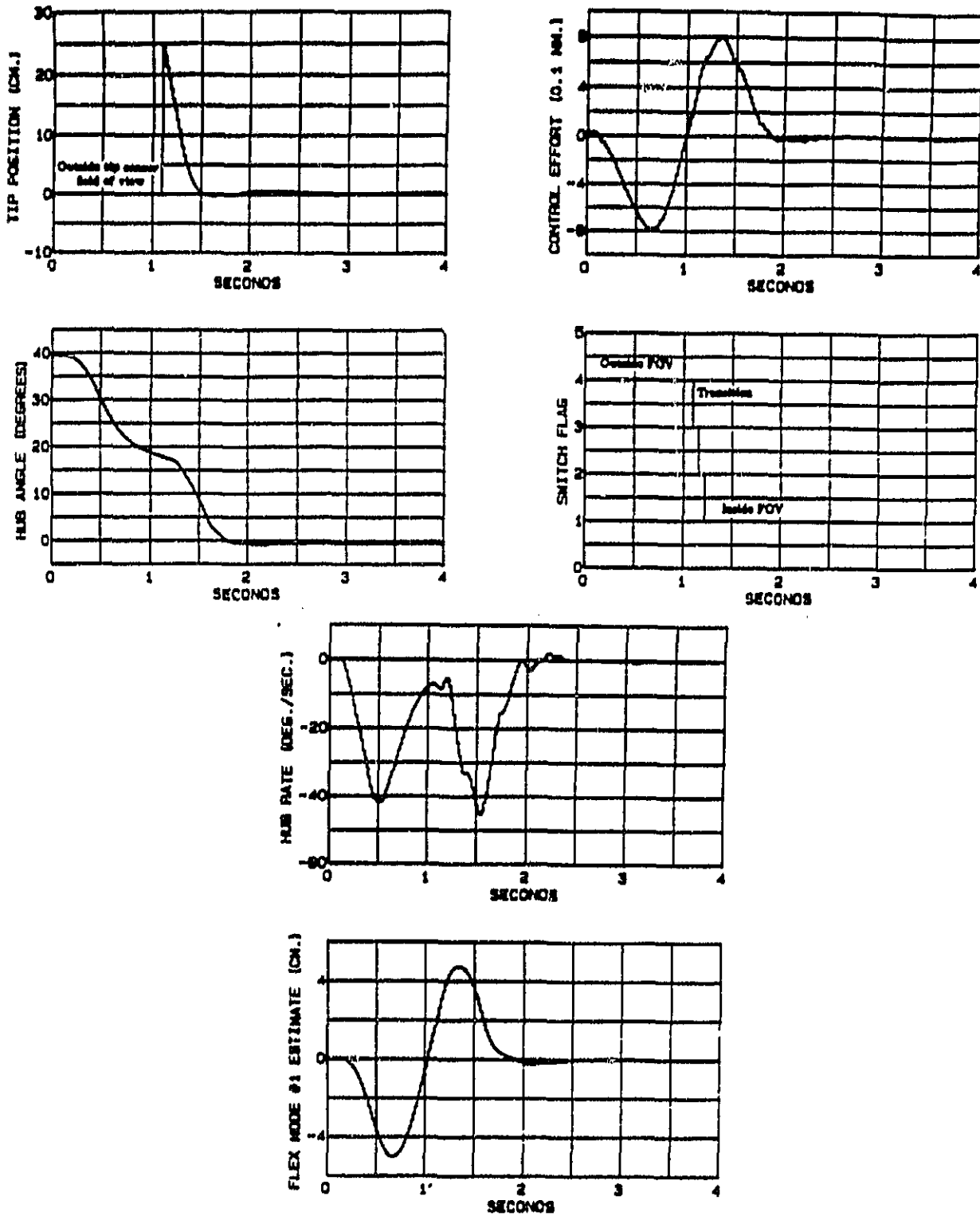


Fig. 6.3 40 degree slow maneuver from outside to inside the tip sensor field of view.

ORIGINAL PAGE IS
OF POOR QUALITY

The main reason for having a set of intermediate gains in the transition region is to alleviate any undesirable torque transient due to an unmodelled difference between the tip sensor and the hub sensor nulls. When the tip of the manipulator comes inside the tip sensor field of view, such a difference corresponds to a step input for the tip compensator. Because it is a double-lead type feedback network, its output will go through a large transient.

The two intermediate gain sets are obtained by varying the ratio of the tip to the hub covariance noise in the same way as in section 4. The sampling rate used for this experiment is 50 Hz. Instead of a current estimator, a predictor estimator is implemented [7]. The reason for this choice is that a current estimator yields a z-plane compensator with direct feedthrough of the sensor signals. Therefore, an unmodelled difference between the tip and hub angle sensor zero readings would create a jump in the torque command. This will be somewhat alleviated for the predictor.

6.4 Regulator and slew command profile

The *unique* regulator gains set is the same as described in section 4.2. For large angle slew maneuvers, a smooth command profile is used instead of a step input u_f . The profile $u_c(\tau)$ is a fifth order spline polynome; its first and second derivative are equal to zero at $t = 0$ and $t = t_f$, where t_f is the slew duration. The expression for u_c is

$$\frac{u_c}{u_f}(\tau) = 6\tau^5 - 15\tau^4 + 10\tau^3$$

$$\tau = \frac{t}{t_f} \quad (26)$$

6.5 Experimental results

We present here a typical recording with the switching algorithm. Figure 6.3 shows a 40 degrees slew maneuver with a commanded duration of 1.2 seconds. The beam is initially positionned outside the tip sensor field of view and is commanded to slew to the middle of the tip sensor field of view. The transition from one gain set to the other is indicated by the switch flag which changes from 4 to 1. The control effort does not exhibit any noticeable transient jumps in the switching region. As shown by the time traces of the first flexible mode estimate (scaled in equivalent tip deflection) and of the hub rate, the arm motion is very different from the one of a rigid body. Nevertheless, the motion of the tip position is well behaved.

7 Conclusion

We have described in some detail the design of a tip position controller using several approaches from classical to modern control theory. It has been shown that colocated rate feedback is a pre-requisite to obtain adequate performance such as high control stiffness for end-point position regulation. Adding a colocated strain gauge makes the feedback system less sensitive to parameter variations and improves the closed-loop disturbance response to external tip forces.¹ Low-order compensators can be designed to obtain performance similar to the LQG method. Modern control methods could be applied to obtain a tip position controller for the linearized dynamics of a multi-link flexible arm.

All the experimental results obtained here began with good knowledge of the flexible arm dynamic parameters. Research needs to be done to extend the experimental work to include adaptive control strategies.

¹We note here that these results are mostly the outcome of having an experimental laboratory set-up, as opposed to pure simulation work.

REFERENCES

- [1] Cannon, R. and Schmitz E., "Initial Experiments on the End-point Control of a One Link Flexible Experimental Manipulator", the International Journal of Robotics Research, The MIT press, Cambridge, Massachusetts, Vol.3, No.3, Fall 1984.
- [2] Schmitz E., "Experiments on the End-Point Position Control of a Very Flexible One-Link Manipulator", PhD Thesis, Stanford University, Dept. of Aeronautics and Astronautics, December 1984.
- [3] Bryson, A.E., "Control theory for random systems," Stanford University, SUDAAR No. 447, Sept. 1972.
- [4] Doyle, J.C., "Robustness with observers," IEEE Trans. on Automatic Control, Vol. AC-24, No.4, August 1979.
- [5] Doyle, J.C., and Stein, G., "Multivariable Feedback Design: Concepts for a Classical/Modern Synthesis," IEEE Trans. on Automatic Control, Vol. AC-26, No.1, February 1981.
- [6] Hall, W.E., and Bryson, A.E., "Optimal Control and Filter Synthesis by Eigenvector Decomposition," Ph.D. thesis, Dept. Aeronautics and Astronautics, Stanford University, Stanford, Ca., SUDAAR No. 436, Nov. 1971.
- [7] Franklin, G.F., and Powell, J.D., Digital control of Dynamic Systems, Addison-Wesley Publishing Co., June 1981.
- [8] Katz, P. and Powell, J.D. "Selection of sampling rate for digital control of aircrafts," Ph.D. thesis, Department of Aeronautics and Astronautics, Stanford University, SUDAAR No. 436, September 1974.
- [9] Ly, U., "A Design Algorithm for Robust Low-Order Controllers," Ph.D. thesis, Department of Aeronautics and Astronautics, Stanford University, SUDAAR No. 536, November 1982.
- [10] Chiang, Wen-wei, Personal communication, Stanford University, 1983.
- [11] Book, W.J., "Modeling, design and control of flexible manipulator arms," Ph.D. thesis, M.I.T., Dept. of Mechanical Engineering, April 1974.
- [12] Hughes, P.C., "Dynamics of a Chain of Flexible Bodies," The Journal of the Astronautical Sciences, Vol.27, No.4, Oct.-Dec. 1979.
- [13] Nguyen, P.K., Ravindran, R., Carr, R. and Gossain, D.M., "Structural flexibility of the shuttle remote manipulator system mechanical arm," Proceedings of the Guidance and Control Conference, AIAA paper No. 82-1536, August 1982.
- [14] Ravindran, R., and Doetsch, K.H., "Design aspects of the shuttle remote manipulator control," Proceedings of the Guidance and Control Conference, AIAA paper No. 82-1581, August 1982.
- [15] Sunada, W.H. and Dubowsky, S. "On the dynamic analysis and behavior of industrial robotic manipulators with elastic members," ASME Design and Production Engineering Technical Conference, Washington D.C., Sept. 12-15 1982, ASME paper 82-DET-45
- [16] Liégois, A., Dombre, E., and Borrel, P., "Learning and control for a compliant computer-controlled manipulator," IEEE Trans. on Automatic Control, Vol. AC-25, No.6, December 1980.
- [17] Usoro, P.B., Nadira, R., Mahil, S.S., "Control of lightweight flexible manipulators: a feasibility study," Proceedings of the American Control Conference, Vol.3, San Diego, California, June 1984.
- [18] Truckenbrodt, A., "Modelling and control of flexible manipulator structures," Proceedings of 4th CISM-IFTOMM Symp. Theory and Practice of Robots and Manipulators, 1981, Warszawa.
- [19] Good, M.C., Sweet, L.M. "Structures for sensor-based robot motion control," Proceedings of the American Control Conference, Vol.1, San Diego, California, June 1984.
- [20] Brady, M., et.al. (ed.), Robot Motion: planning and control The MIT press, Cambridge, Massachusetts, 1982.
- [21] Lacombe, J.L., Berger, G., "In-space assembly and maintenance of unmanned spacecraft," Proceedings of the International Federation of Automatic Control in Space, Noordwijkerhout, The Netherlands, 1982.
- [22] Gran, R., "Control of flexible structures: a systematic overview of the problems," Proceedings of the Workshop on Applications of Distributed System Theory to the Control of Large Space Structures, Rodriguez, G. (Editor), JPL Publication 83-46, NASA, July 1983.
- [23] Schaechter, D.B., "Hardware demonstration of flexible beam control," Journal of Guidance and Control, Vol.5, No.1, January 1982.
- [24] Breakwell, J.A., Chambers, G.J., "The Toysat structural control experiment," The Journal of the Astronautical Sciences, Vol. 31, No.3, July-September 1983.
- [25] Bauldry, R.D., Breakwell, J.A., Chambers, G.J., Jolkansen, K.F., Nguyen, N.C. and Schaechter, D.B., "A hardware demonstration of control for a flexible offset-feed antenna," The Journal of the Astronautical Sciences, Vol. 31, No.3, July-September 1983.

Appendix A

Flexible arm open-loop transfer functions

This appendix gives the open-loop s -plane transfer functions from torque input T to sensors outputs. They are obtained with a computer code (Optsys) from the equations (3) and Table 1 of section 2. Open-loop transfer functions are useful for understanding the basic characteristics of the control problem at hand, and also for control design with the root-locus and Bode plot methods.

Colocated hub angle sensor (in units of Rads per Nm)¹

$$\frac{\theta(s)}{T(s)} = \frac{46.32}{s(s+0.2)} \frac{((s+0.1)^2 + 3.4^2)}{((s+0.2)^2 + 11.79^2)} \frac{((s+0.29)^2 + 17.47^2)}{((s+0.4)^2 + 21.6^2)} \frac{((s+1.15)^2 + 46.42^2)}{((s+1.2)^2 + 48.05^2)} \quad (1)$$

Colocated pseudo hub rate angle sensor (in units of Rads/sec per Nm)

$$\frac{\dot{\theta}(s)}{T(s)} = \frac{64.7}{s+64.7} \frac{\theta(s)}{T(s)} \quad (2)$$

Tip position sensor (in units of m per Nm)

$$\frac{y_t}{T(s)} = -\frac{2.177}{s(s+0.2)} \frac{(s+12.05)(s-12.13)}{((s+0.2)^2 + 11.79^2)} \frac{((s+22.2)^2 + 24.1^2)((s-21.6)^2 + 25.44^2)}{((s+0.4)^2 + 21.6^2)((s+1.2)^2 + 48.05^2)} \quad (3)$$

Nearly colocated strain-gauge sensor

$$\frac{\epsilon_1(s)}{T(s)} = 79.86 \frac{((s+0.2)^2 + 13.7^2)((s+0.9)^2 + 39.12^2)((s+1.15)^2 + 46.42^2)}{((s+0.2)^2 + 11.79^2)((s+0.4)^2 + 21.6^2)((s+1.2)^2 + 48.05^2)} \quad (4)$$

¹The Laplace variable s is in units of Rad/sec.

Appendix B

Locus of asymptotic estimator poles

This appendix explains the derivation of the three root-loci given in section 5.2 of chapter 5. The poles of the steady-state continuous Kalman filter are the roots of the characteristic equation

$$\det\{R + qZ(s)Z^T(-s)\} = 0 \quad (1)$$

where R is a diagonal matrix with strictly positive elements ($R_{v_1}, R_\theta, R_{\epsilon_1}$) and q is a positive real number corresponding to the process noise covariance.

$Z(s)$ is a column vector which consists of the three open-loop transfer functions for the sensors mounted on the beam.

From the general relation valid for two arbitrary matrices A and B ,

$$\det\{I_n + A_{n,m}B_{m,n}\} = \det\{I_m + B_{m,n}A_{n,m}\} \quad (2)$$

equation (1) can be expressed as

$$1 + qZ^T(-s)R^{-1}Z(s) = 0 \quad (3)$$

if $H_x(s)$ is the open-loop transfer function for sensor x , equation (3) becomes

$$1 + \frac{q}{R_{v_1}} \bar{f} \bar{v}_i(s) H_{v_i}(-s) + \frac{q}{R_\theta} H_\theta(s) H_\theta(-s) + \frac{q}{R_{\epsilon_1}} H_{\epsilon_1}(s) H_{\epsilon_1}(-s) = 0 \quad (4)$$

With the notation: $H_x(s) = \frac{N_x(s)}{D(s)}$, we obtain

$$1 + \frac{q}{R_{v_1}} \frac{1}{D(s)D(-s)} \{N_{v_1}(s)N_{v_1}(-s) + \frac{R_{v_1}}{R_\theta} (-s^2)N_\theta(s)N_\theta(-s) + \frac{R_{v_1}}{R_{\epsilon_1}} s^4 N_{\epsilon_1}(s)N_{\epsilon_1}(-s)\} = 0 \quad (5)$$

Let the ratio $\frac{q}{R_{v_1}}$ go to infinity.

Given the ratios $\frac{R_{v_1}}{R_\theta}$ and $\frac{R_{v_1}}{R_{\epsilon_1}}$, the finite estimator poles will tend asymptotically toward the stable zeroes of the quantity between brackets in equation (5).

Let us first consider the case where the strain-gauge 1 is not used, i.e. $\frac{R_{y1}}{R_{t1}} = 0$. Then, from (5), the finite estimator poles belong to the Evans root-locus whose characteristic equation is

$$1 + \frac{R_{y1}}{R_{\theta}}(-s^2) \frac{N_{\theta}(s)N_{\theta}(-s)}{N_{v1}(s)N_{v1}(-s)} = 0 \quad (6)$$

When the strain-gauge 1 is used, and if we fix the ratio $\frac{R_{y1}}{R_{\theta}}$, the estimator poles belong to the Evans root-locus given by

$$1 + \frac{R_{y1}}{R_{t1}} s^4 \frac{N_{t1}(s)N_{t1}(-s)}{N(s)N(-s)} = 0 \quad (7)$$

where $N(s)$ is defined as

$$N(s)N(-s) = N_{v1}(s)N_{v1}(-s) + \frac{R_{y1}}{R_{\theta}}(-s^2)N_{\theta}(s)N_{\theta}(-s) \quad (8)$$

This derivation is valid only for a single-input multi-outputs system. It would be useful to derive an algorithm to test the existence and obtain the location of the finite estimator poles of a MIMO system.

Appendix C

Transfer function calculations

In this appendix, we explain how to obtain the actuator loop and tip loop transfer functions discussed in section 4.4.3.

The dynamic system equations of order ns are

$$\begin{aligned} \dot{x} &= Fx + Gu \\ y &= Hx \end{aligned} \quad (1)$$

where y are the ns sensor outputs, and u is the control input (only one input for our case). The corresponding open-loop transfer function matrix is

$$G(s) = H(sI_{ns} - F)^{-1}G \quad (2)$$

The compensator dynamic equations of arbitrary order r are¹

$$\begin{aligned} \dot{z} &= Az + By \\ u &= C_r z \end{aligned} \quad (3)$$

For the case discussed in this report, the matrix B is made-up of three column vectors, B_{y_1} , B_{c_1} , B_θ

The corresponding open-loop compensator transfer function is

$$K(s) = C_r(sI_{ns} - A)^{-1}B$$

The quantity $K(0) = -CA^{-1}B_{y_1}$ is the steady-state tip compensator gain which is one of the performance measures for the tip position closed-loop system as shown in section 4.4.3.

For the case of an LQG compensator, the matrices A , B , C_r are respectively

¹We assume here that the compensator does not have any direct transmission term from sensor output to control input.

$$\begin{aligned}
 A &= F - GC - KH \\
 B &= K \\
 C_r &= C
 \end{aligned}
 \tag{4}$$

where K and C are respectively the steady-state filter gain and full-state feedback gain matrices.

The actuator loop transfer function, commonly called $G(s)K(s)$, is obtained as the open-loop transfer-function for the system $(\tilde{A}, \tilde{B}, \tilde{C})$ of order $ns + r$, where

$$\begin{aligned}
 \tilde{A} &= \begin{bmatrix} F & \mathbf{O} \\ BH & A \end{bmatrix} & \tilde{B} &= \begin{bmatrix} G \\ \mathbf{O} \end{bmatrix} \\
 \tilde{C} &= (\mathbf{O} \quad C_r)
 \end{aligned}
 \tag{5}$$

For the system discussed in this report, $G(s)K(s)$ is a single-input single-output transfer function, because only one actuator is used. Therefore, we used a simple Bode plot to discuss the stability of the closed-loop system with respect to actuator dynamics.

In the same fashion, the tip position loop transfer function (with the hub rate and strain-gauge sensors loops closed) is obtained as the open-loop transfer function for the system $(\tilde{A}, \tilde{B}, \tilde{C})$ of order $ns + r$, where

$$\begin{aligned}
 \tilde{A} &= \begin{bmatrix} F & GC_r \\ B_\delta H_\delta + B_{c_1} H_{c_1} & A \end{bmatrix} & \tilde{B} &= \begin{bmatrix} \mathbf{O} \\ B_{y_1} \end{bmatrix} \\
 \tilde{C} &= (H_{y_1} \quad \mathbf{O})
 \end{aligned}
 \tag{6}$$

Again, we obtain a single-input single-output transfer function.

Appendix D

Discrete LQG compensator implementation and check-out

1 LQG compensator implementation

This section is based on Franklin and Powell, Ref. [7] (p148 and p 160-161). For our particular application, we choosed to implement a current estimator instead of a predictor estimator. This is because only a small amount of sensor data processing needs to be done before the feedback control signal can be sent to the D to A board. For other applications involving many sensors and actuators, only a predictor estimator could be implemented. The order of the estimator is ns , the number of sensors is nz and there is only one actuator. Given the zero-order hold discrete equivalent (Φ and Γ)¹ of the open-loop system matrices (F and G), the current estimator equations are

$$\begin{aligned}x(k+1) &= \Phi \hat{z}(k) + \Gamma u(k) \\ \hat{z}(k) &= z(k) + K(z(k) - Hz(k))\end{aligned}\quad (1)$$

where K are the discrete current estimator gains.² Given the discrete steady-state regulator gains C , the control signal u_k is computed according to

$$u(k) = C \hat{z}(k) \quad (2)$$

As it is shown in Reference 7, the equations (1) and (2) can be recast into a general compensator form which is the one we choosed to implement. Actually, we used a slightly modified form in order to implement actuator torque saturation limits. These equations are the following

$$\begin{aligned}x_c(k+1) &= Ax_c(k) + B_u u(k) + B_z z(k) \\ u(k) &= Cx_c(k) + Dz(k)\end{aligned}\quad (3)$$

¹ Φ is set into modal form according to the dynamics model given in section 2.

²the notation K for the filter gains is used instead of L .

```

Read sensor data from A to D
Substract D.C. bias
Check if inside tip sensor Field Of View
Compute control command :
     $u = u_{com} + \bar{u} + D_1 y_1 + D_2 \dot{\theta} + D_3 \epsilon_1$ 
Saturate command u if  $|u| > u_{sat}$ 
Output u on D to A
Do equation update (3)
If desired, store sensor data in arrays
Return to background & wait for next clock tick
    
```

Fig. 1 LQG control algorithm implementations:

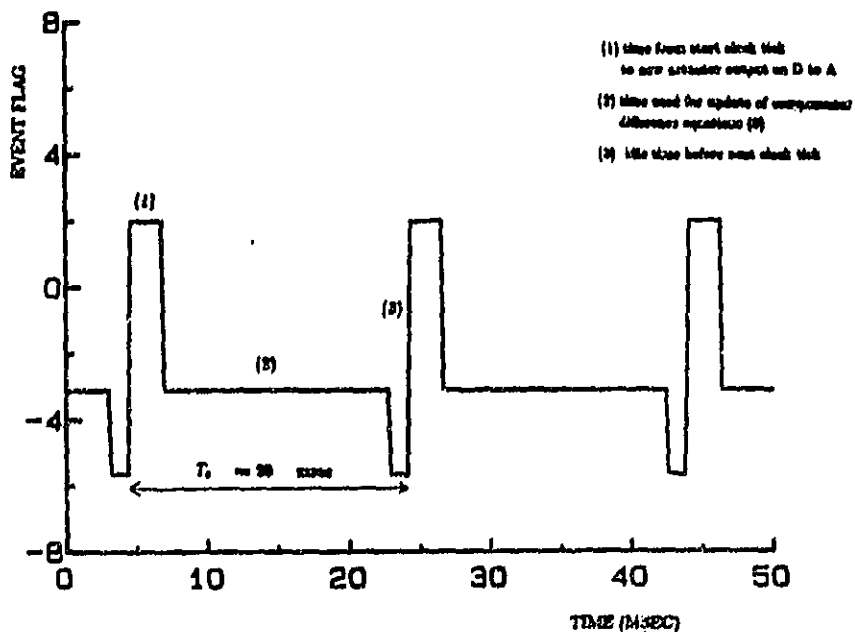


Fig. 2 Typical durations for real-time controller implementation:

with the following definitions:

$$\begin{aligned}x_e(k) &= \hat{x}(k) - Kx(k) \\ A &= (I_{n_s} - KH)\Phi \\ B_e &= (I_{n_s} - KH)\Gamma \\ B_x &= (I_{n_s} - KH)\Phi K \\ D &= CK\end{aligned}\tag{4}$$

Implementing equations (3) takes $3ns$ less multiplication operations than implementing equations (1) and (2). With equation (3), $ns \times nx$ more multiplications are needed in addition if we want to compute the state estimate $\hat{x}(k)$ for checking purposes.

The block diagram shown in Figure 1 gives an overview of the control algorithm implemented on the computer. Figure 2 shows how much time is necessary to perform each of the above operations on the Minc 11 DEC laboratory computer, with the operating system RT11.V04 (floating point hardware). As shown in Figure 2, the sampling period is 20 msec. The LQG compensator is 9th order with 3 sensors inputs. Between two successive clock ticks, there is about 1.4 msec of idle time left, which can be used for data storage for latter plotting. Note that all the code is written in Fortran and no particular effort was done for speed optimization.

2 Compensator check-out

This section is a potpourri of obvious checks which should be useful only for the unexperienced experimental control systems engineer.

0) first commandment

When testing an active control system on an expensive mechanical system that can undergo substantial elastic deformations under the action of its controlled actuator, it is highly recommended to use on-off switches at several convenient locations close to the experiment.¹ Safety is also an important consideration as we are concerned here with manipulators of relatively large sizes.

1) zero in = zero out

That is, if we ground all the inputs to the compensator (A to D bnc's), the control signal output should be zero (D to A bnc).

2) check compensator transfer function

First, check that the *sign* of the compensator is correct: for a minimum phase compensator, a positive sensor input (with all the other sensor inputs grounded) should produce a negative torque command for the actuator (assuming everything follows a given positive sign convention). The D.C. gain from a given input of the compensator to the control signal output can easily be checked with its theoretical value. For frequencies which are much below the Nyquist rate, we can perform a frequency response test and compare the gain/phase Bode plot with the one

¹As a corollary, if nothing happens when the experimentator turns on the closed-loop feedback system, the most likely explanation is that the kill switch has not been reset, or the power has not been turned on.

predicted by the analysis. Another method is to compare the step response of the experimental compensator (from a given input to the control output) with the theoretical one.

These checks can only be done if the compensator has stable poles. When designing an LQG compensator for the flexible arm, we found that sometimes the resulting compensator would have some poles slightly unstable, especially for the case of colocated hub angle and hub rate LQG compensators. At least, for a slightly unstable compensator, one can check if the frequency of the slowly unstable mode agrees with the one predicted by the theory.¹ The personal opinion of this writer is that unstable compensators are basically unsafe as far as practical implementation goes.

A properly designed LQG compensator should result in a closed-loop system with adequate stability margins. Nevertheless, if one of the feedback loop is opened, the resulting system is not necessarily stable. For the case of the flexible arm, the rate loop for the tip and hub rate LQG compensator designed in section 3 has some lightly damped closed-loop poles. This might not be always desirable for a manipulator system. It might be possible to choose other weighting matrices or modify the design procedure so that the closed-loop poles are more damped.

3) miscellaneous

It is wise to have a variable loop gain in front of the computed control signal which is sent to the D to A board. If the closed-loop system is unstable, we can try again with a loop gain reduced by two, and so on and so on...

If the closed-loop system presents a small amplitude limit cycle, here are a few things to look at:

1. actuator non-linearities: friction and cogging torque. One possible solution is to use a high rate loop around the actuator so that the effective friction level are reduced.
2. poor phase margin: if for instance the actuator loop ($G(s)K(s)$) has a small phase margins (10 degrees or less), it is possible to get a closed-loop limit cycle resulting from non-linear dynamics (friction) and unmodelled phase lags such as actuator dynamics and computational delays (between sensors data readings and control signal output).
3. sensor noise aliasing: the sensor noise spectrum can be aliased by the computer sampling process in low frequency signal which can be amplified by the compensator transfer function resulting in an unwanted limit cycle. One simple test is to change the sampling rate: the frequency of the limit cycle should change accordingly.

When the controlled output is zero (i.e. the tip position sensor for the flexible arm), it should remain at zero as long as the control system is on. If it changes with time, one has to look for sensors drifts. One can easily obtain for each sensor used for feedback the sensitivity factor defined as the ratio of change in controlled output to change in a given sensor signal D.C. bias (this is for the case where we do not have integral control).

ORIGINAL FILED
OF FOUR VOLUMES

¹It is quite an experience to let the controller run open-loop unstable for a few hundred milliseconds and then to close the loop with the flexible arm to obtain a resulting stable system!